

THE BANARAS METALLURGIST

VOL. 19

2014

The Banaras Metallurgist

CHIEF EDITOR

G.V.S. Sastry

MANAGING EDITOR

V. Jindal

EDITORIAL BOARD

T.R. Mankhand	Member
S.N. Ojha	Member
R.K. Mandal	Member
N.K. Mukhopadhyay	Member
S. Mohan	Member
N.C. Santhi Srinivas	Member
B.N. Sarma	Member
I. Chakrabarty	Member

EDITORIAL ADVISORY BOARD

C. Suryanarayana	Member
S. Lele	Member
G.M.K. Sarma	Member
Mohd. Shamsuddin	Member
V. Jayaram	Member
I. Manna	Member
S. Srikanth	Member
B.S. Murty	Member
P.M. Ajayan	Member
U. Ramamurty	Member
S. Sampath	Member

STUDENT EDITOR

Rahul Gupta	B.Tech. Part – IV
Sarvesh Mundra	IDD Part – III

EDITORIAL OFFICE

Head of Department
Dept. of Metallurgical Engineering
Indian Institute of Technology
(Banaras Hindu University)
Varanasi 221005, India.

Telephone : 0542-2369478, 2369346
Telefax : 0542-2369478
Email : head.met@iitbhu.ac.in

An Organ of the

METALLURGICAL SOCIETY, BHU

Supported by

Professor N.P. Gandhi Memorial Metallurgy Trust

THE BANARAS METALLURGIST

The Banaras Metallurgist is an annual technical journal covering all aspects of metals and materials. This journal is being published since 1968 and it has made its position in India and abroad as evidenced by the citations.

Vol. 19

2014

Displacements Caused by the Growth of Bainite in Steels

H.K.D.H. Bhadeshia

Materials Science and Metallurgy, University of Cambridge, U. K., hkdb@cam.ac.uk

Abstract

One of the important characteristics of solid-state phase transformations in steels is the choreography of atoms as they traverse the frontier between the parent and the product phases. Some transformations involve a chaotic motion of atoms consistent with long-range diffusion, and hence are closer to equilibrium than those that where a disciplined transfer occurs. Since the pattern of atoms changes during transformation, a disciplined motion of atoms necessarily leads to a change in the shape of the transformed region, and like any deformation, such changes cause strains in the surrounding material. These displacive transformations are therefore strain dominated, with the morphology, chemical composition and thermodynamic framework sensitive to the strain energy due to the shape change. Here we consider the published data that have been accumulated on the displacements associated with 'bainite', a phase transformation product in steels that forms the basis of the world's first bulk nanocrystalline metal.

Introduction

There are two reasons for writing this paper, the first being to demonstrate how the movement of atoms during a change in crystal structure can be recorded, and the second to emphasise the nature of bainite in steels – after all, it is the fine bainite that remains the only commercial success in the field of nanostructured materials used in large-scale engineering applications.

There are two essential kinds of solid-state phase transformations in metals and alloys. Reconstructive transformations involve the uncoordinated motion of atoms, with diffusion occurring to minimise the strain energy of transformation, and in the case of alloys, to facilitate the partitioning of solutes between the parent and product phases until the chemical potential of each component becomes uniform across the phases.

The second kind involves a homogeneous deformation of the parent structure into that of the product; atoms on the substitutional lattice do not diffuse during transformation. The deformation causes a change in the shape of the transformed region, a change that can be measured and related to the atomic mechanism of transformation [1, 2]. Transformations like these involve macroscopic displacements and hence are labelled 'displacive'.

There is additional complexity in the case of steels, where the crystal structure is described in

terms of the iron and substitutional-solute atoms, whereas the carbon that resides in interstices between the large atoms and in displacive transformations is chaperoned into the new lattice. On the other hand, the greater mobility of the carbon atoms means that they can partition while the substitutional lattice is displaced [3]; but their diffusion has no consequence on the shape deformation accompanying the crystal structure change [3].

Throughout this paper, the parent phase is austenite, with a cubic close-packed crystal structure, and the product phase is bainitic ferrite, whose structure is conventionally regarded as body-centred cubic but can also have lower symmetry depending on the carbon that is present in solid solution [4–6]. Bainite is a displacive transformation and one which is of immense technological importance [7–9]. All of the characteristics that make bainite so useful rely on the fact that it is a strain dominated transformation. Thus, the morphology and size of the bainite plates depend on the minimization of strain energy due to the shape deformation. The shape deformation is an invariant-plane strain, i.e., one which leaves a plane macroscopically unrotated and undistorted [10, 11]; the invariant-plane is also the one on which the bainite plates lengthen. In detail, the shape deformation consists of a large shear on the invariant plane and a small dilatation normal to that plane, as

illustrated schematically on Fig. 1, which also shows an actual image of the displacements produced when a single crystal of austenite is polished flat and allowed to transform into plates of bainite. This deformation creates a large dislocation density in the austenite, that in turn opposes the motion of the transformation interface [12], which mechanically stabilises the austenite [13] and hence stops the bainite platelets from coarsening.

The purpose of this paper is to assemble the data on measurements of the shape deformation of bainite, and to assess their value. We begin first with a description of the consequences of the shape deformation so that the measurements can be placed in context. As will be seen later, the measurements concerned are difficult and have to be conducted at a variety of resolutions.

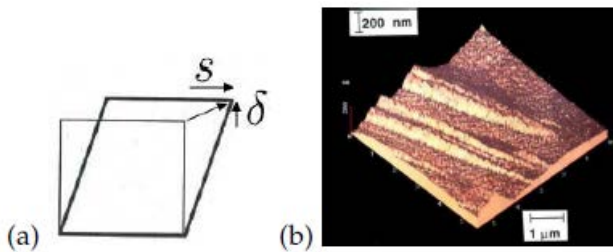


Figure 1. (a) Schematic illustration of a general invariant plane strain defined by the cube of unit height changing into a parallelepiped. s and δ represent the shear and dilatational strains respectively. The combination of s and δ leads to the displacement m that is not parallel to the habit plane (the horizontal invariant plane). (b) Actual shape change due to individual platelets of bainite [14].

Consequences of Shape Deformation

Why is the shape deformation important in the theory and practice of solid-state phase transformations? Like any deformation that occurs within a metal, the material surrounding the individual plate is required to accommodate the displacements. In other words, compatibility requires that there are distortions in the matrix around each plate of bainite. For an elastically accommodated, isolated plate in the form of an oblate spheroid with length r much greater than the thickness c , located within elastically isotropic

austenite, the strain energy per unit volume is given by [15]:

$$G_{\text{strain}} = \frac{c}{r} \frac{\mu}{1-\nu} \left[\frac{\pi}{4} \delta^2 + \frac{\pi}{8} (2-\nu) s^2 \right] \approx \frac{c}{r} \mu (s^2 + \delta^2) \quad (1)$$

where μ and ν are the respective shear modulus and Poisson's ratio of austenite, and s and δ are respectively the shear and dilatational strains parallel and normal to the habit plane. For bainite, this strain energy comes to about 400 Jmol^{-1} [16], which is large in the context of the chemical free energy change accompanying transformation to say allotriomorphic ferrite or pearlite. G_{strain} therefore dominates the bainite reaction, and is the sole reason why the product is in the form of thin plates ($c \ll r$) because a small aspect ratio minimises the strain energy. This of course is the same reason why martensite and mechanical twins form as thin plates.

Bainite forms at temperatures where the parent austenite is not strong. As a result, the shape deformation during transformation causes plastic relaxation in the adjacent austenite. The dislocation debris thus created in the austenite then opposes further transformation by a phenomenon known as mechanical stabilisation [17–22], and brings the growth of a plate to a halt before it impinges with hard obstacles [13]. This has technological consequences because it leads to a dramatic refinement of the structure, and the increase in dislocation density contributes to strength.

Disciplined movements of atoms cannot in general be sustained across crystal boundaries, so unlike diffusional transformations, plates of bainite are restricted to grow within the grains in which they nucleate.

The Data

Qualitative data

The very first observation of the shape deformation due to clusters of bainite plates was by Ko and Cottrell [23]; a pre-polished sample of austenite was transformed into bainite and the resulting upheavals at the surface measured by traversing a stylus across the surface (Fig. 2a). The horizontal resolution is of the order of a few micrometers, which compares with a typical plate thickness of $0.25 \mu\text{m}$. The work nevertheless had a profound effect on the

development of the subject because it identified the first evidence for the disciplined movement of atoms involved in the growth of bainite.

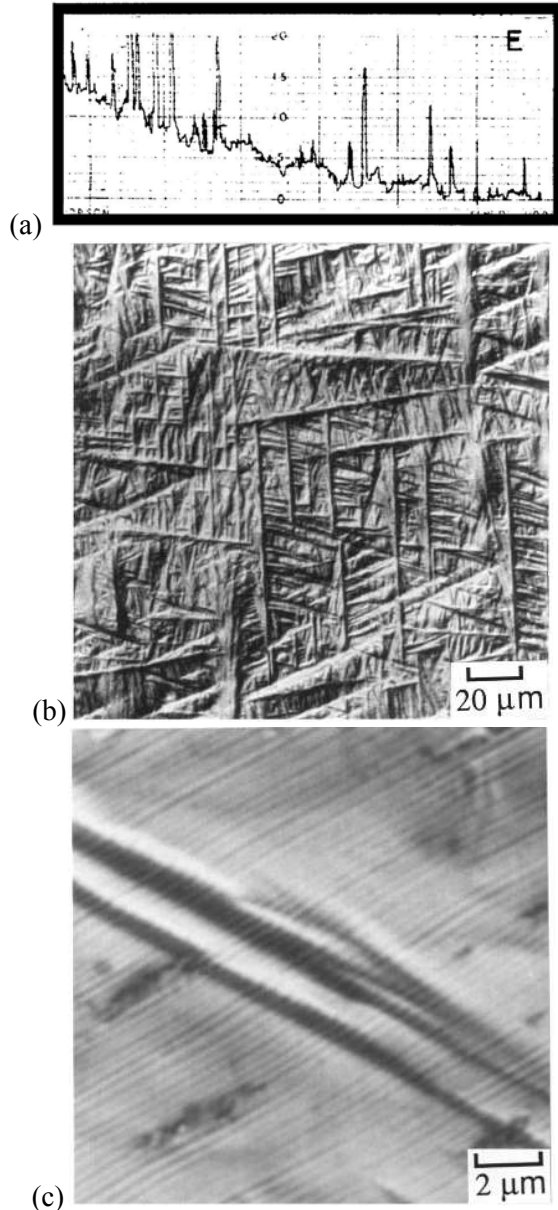


Figure 2. (a) Stylus record of surface upheavals caused by the bainite transformation. The horizontal graduations correspond to 1/100 of an inch, and the vertical magnification is ten times greater [23]. (b,c) Nomarski interference micrographs showing at a greater resolution, the displacements caused on a pre-polished sample of austenite by the formation of bainite [16].

Speich [24] subsequently used the surface relief to follow the growth kinetics of clusters of bainite plates using hot-stage optical microscopy, but did not report quantitative data on the nature of the relief. Somewhat higher resolution data obtained using Nomarski interference optical microscopy are shown in Fig. 2b,c.

Quantitative data

None of the above measurements gave a quantitative value to the shape deformation of bainite. This is because light microscopy does not have the resolution to reveal the displacements due to individual platelets (the so-called sub-units of the transformation, [25]). Measurements of the shear strain using scratch displacements have the same resolution problem. The phases separating the bainitic ferrite sub-units have the effect of reducing the overall shear since they are benign during transformation. Srinivasan and Wayman realised that the shear strain data they measured using scratch displacements (Table 1) are likely therefore to be underestimates of the actual shear; comparison with crystallographic theory indicated that the actual shear strain should be about twice that measured.

Table 1. Magnitude of the shear strain averaged over a collection of bainite platelets containing also undeformed austenite [26].

Angle of shape shear	Shear strain s
7°9'	0.1254
8°27'	0.1254
7°0'	0.1254
7°55'	0.1254
8°20'	0.1254
5°13'	0.1254
8°24'	0.1254
6°	0.1254

An ingenious observation by Sandvik confirmed that the true shear is $s \approx 0.22$; the measurement relied on the deflection caused by the shape deformation of bainite, of twins present in the austenite, and observed using thinfoil transmission electron microscopy (Fig. 3).

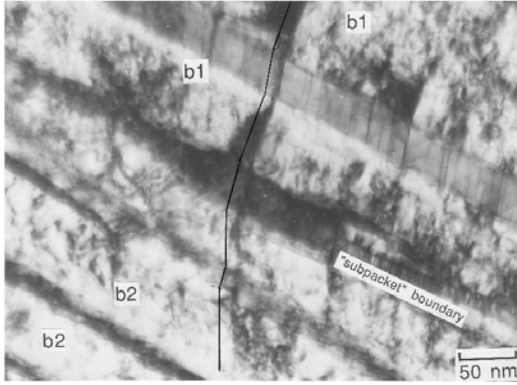


Figure 3. Displacement of twin boundaries caused by individual sub-units of bainite. The ferrite variants 'b1' and 'b2' belong to separate sheaves [27].

Atomic force microscopy (AFM) has the ability to resolve the displacements due to individual sub-units (Fig. 1b) and has provided considerable detail on the plastic accommodation effects caused in the adjacent austenite. Fig. 4 shows the plastic relaxation of the austenite adjacent to the bainitic ferrite. As emphasized earlier, it is important to measure the displacements due to individual platelets rather than that of a cluster of sub-units with intervening phases.

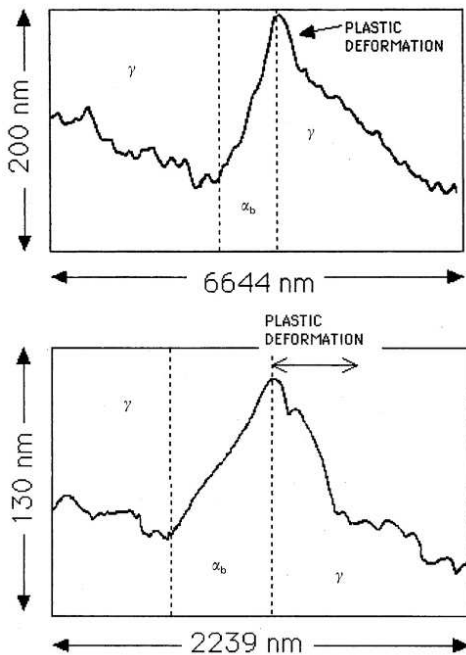


Figure 4. Atomic force microscope scans across individual bainite sub-units showing the plastic deformation in the austenite (γ) adjacent to the bainitic ferrite (α_b) [14].

AFM on its own does not give information about the orientation of the plate under the surface. Therefore, all measurements of the shear strain are *apparent*, dependent on the inclination of the plate and displacement direction relative to the free surface. Such data are illustrated in Fig. 5 for a number of measurements, with the shaded region representing reported values calculated using the crystallographic theory of displacive transformations [28–31]. The largest recorded value of the apparent shear is 0.26, with the relevant displacements shown in Fig. 6. This can be taken as the *minimum* value of the true shear, with $s \geq 0.26$. This is a large strain, far greater than a typical elastic strain of just 10–3, and its consequence, particularly on the associated strain energy (equation 1), should not be neglected in thermodynamic or kinetic assessments of the bainite transformation.¹

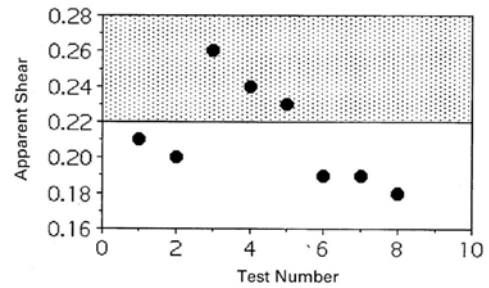


Figure 5. AFM measurements of the apparent shear caused by the growth of bainite [14]. The largest apparent shear is the minimum value of the true shear.

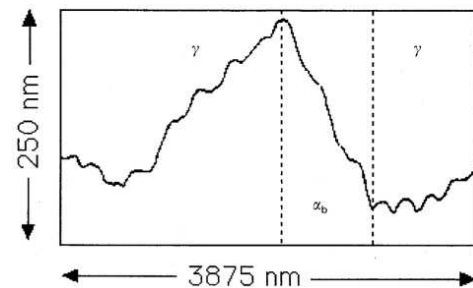


Figure 6. An AFM scan showing an apparent shear strain of 0.26 caused by the growth of a bainite sub-unit [14].

1. Reported scanning tunnelling microscopy data [32–34] on the surface relief caused by bainite are unfortunately of insufficient quality and lack quantitative interpretation to warrant detailed discussion.

There has been much confusion on the microstructure of thermomechanically processed low-carbon (0.05wt%) and high-niobium (0.1wt%) pipeline steels, many millions of tonnes of which have been manufactured for the transmission of fossil fuels. It appears, however, that the confusion arises because insufficient parameters have been investigated in the published literature to enable the mechanisms to be resolved. A recent investigation has shown that the structure is correctly described as bainite [35]. The surface relief data listed in Table 2 are consistent with this, and with $s \geq 0.26$.

Table 2. Apparent shear component (s_a) of shape deformation due to the growth of bainite platelets, [35].

Sample	Measured s_a	Sample	Measured s_a
1	0.18	4	0.24
2	0.19	5	0.24
3	0.24	6	0.17

More recent work on nanostructured bainite that typically forms during transformation at 200°C [36], has found that the shear strain associated with the slender plates of bainitic ferrite can be even larger at $s \geq 0.46$, [36], Table 2. This would, on the basis of equation 1, explain why the plates are only 20-40 nm in thickness. However, there is as yet no explanation of why the crystallography of the nanostructured bainite should be different from that of coarser bainite obtained at higher temperatures.

Summary

The fact that there is an invariant-plane shape change generated when austenite transforms into bainite is well established. It is also clear that the shear component of this shape deformation is large, with a minimum value of 0.26. Such a shape deformation should not be neglected when considering the mechanisms of phase transformation, as is often done, even in modern literature [37, 38, e.g.].

Perhaps it is more constructive to identify what remains to be done with respect to the displacive nature of the bainite reaction. The theoretical background to the crystallography of displacive reactions can be summarized as follows [28–31]:

$$P_1 P_2 = RB$$

where B is the Bain strain is the pure deformation that converts the crystal structure of austenite into ferrite, R is the rigid body rotation that in combination with B gives a total deformation that leaves a line invariant. The existence of such a line is a necessary condition for martensitic transformation [11, 39]. The RB at the same time predicts the observed orientation relationship. P_1 is the shape deformation matrix representing the invariant plane strain and P_2 is a lattice-invariant deformation that could be slip or twinning. The plane on which P_1 occurs is of course the habit plane of the bainite in the present context. The point that emerges from this equation is that the shape deformation, orientation relationship and the crystallographic indices of the habit plane are all connected mathematically. All three of these quantities have been measured independently or as incomplete sets, but there has never been an experiment where they have been simultaneously determined for an individual bainite sub-unit. The reason of course is that this would be a difficult experiment given the fine scale of the subunit, but modern techniques including combination of atomic force microscopy, focused-ion beam machining and transmission electron microscopy could resolve the problem and bring closure to the subject.

The second issue highlighted here is the plastic accommodation of the shape deformation. Although the mechanical stabilisation of the austenite due to this effect is resolved quantitatively [13], it is not clear how the plastic accommodation influences the development of the crystallography of bainite.

References

- [1] J. W. Christian, "Lattice correspondence atomic site correspondence and shape change in diffusional displacive phase transformations," *Progress in Materials Science*, vol. 42, pp. 109–124, 1997.
- [2] H. K. D. H. Bhadeshia, *Bainite in Steels*, 2nd edition. London, U.K.: Institute of Materials, 2001.
- [3] J.W. Christian, "The origin of surface relief effects in phase transformations," in *Decomposition of austenite by diffusional processes*, V. F. Zackay and H. I. Aaronson, Eds. New York, USA: Interscience, 1962, pp. 371–386.

- [4] J. H. Jang, H. K. D. H. Bhadeshia, and D. W. Suh, "Solubility of carbon in tetragonal ferrite in equilibrium with austenite," *Scripta Materialia*, vol. 68, pp. 195–198, 2012.
- [5] C. N. Hulme-Smith, I. Lonardelli, A. C. Dippel, and H. K. D. H. Bhadeshia, "Experimental evidence for non-cubic bainitic ferrite," *Scripta Materialia*, vol. 69, pp. 409–412, 2013.
- [6] H. K. D. H. Bhadeshia, "Carbon in cubic and tetragonal ferrite," *Philosophical Magazine*, vol. ?, p. <http://dx.doi.org/10.1080/14786435.2013.775518>, 2013.
- [7] F. B. Pickering, "The structure and properties of bainite in steels," in *Transformation and hardenability in steels*. Michigan, USA: Climax Molybdenum Co., 1967, pp. 109–132.
- [8] F. G. Caballero, H. K. D. H. Bhadeshia, K. J. A. Mawella, D. G. Jones, and P. Brown, "Very strong, low-temperature bainite," *Materials Science and Technology*, vol. 18, pp. 279–284, 2002.
- [9] H. K. D. H. Bhadeshia, "The first bulk nanostructured metal," *Science and Technology of Advanced Materials*, vol. 14, p. 014202, 2013.
- [10] J. W. Christian, *Theory of Transformations in Metals and Alloys, Part I*, 3rd ed. Oxford, U. K.: Pergamon Press, 2003.
- [11] —, *Theory of Transformations in Metals and Alloys, Part II*, 3rd ed. Oxford, U. K.: Pergamon Press, 2003.
- [12] H. K. D. H. Bhadeshia and D. V. Edmonds, "The bainite transformation in a silicon steel," *Metallurgical Transactions A*, vol. 10A, pp. 895–907, 1979.
- [13] S. Chatterjee, H. S. Wang, J. R. Yang, and H. K. D. H. Bhadeshia, "Mechanical stabilisation of austenite," *Materials Science and Technology*, vol. 22, pp. 641–644, 2006.
- [14] E. Swallow and H. K. D. H. Bhadeshia, "High resolution observations of displacements caused by bainitic transformation," *Materials Science and Technology*, vol. 12, pp. 121–125, 1996.
- [15] J. W. Christian, "Accommodation strains in martensite formation, the use of the dilatation parameter," *Acta Metallurgica*, vol. 6, pp. 377–379, 1958.
- [16] H. K. D. H. Bhadeshia and D. V. Edmonds, "The mechanism of bainite formation in steels," *Acta Metallurgica*, vol. 28, pp. 1265–1273, 1980.
- [17] M. J. C. J. R. Strife and G. S. Ansell, "Effect of austenite prestrain above the Md temperature on the Ms temperature in Fe-Ni-Cr-C alloys," *Metallurgical Transactions A*, vol. 8A, pp. 1471–1484, 1977.
- [18] P. H. Shipway and H. K. D. H. Bhadeshia, "Mechanical stabilisation of bainite," *Materials Science & Engineering A*, vol. 11, pp. 1116–1128, 1995.
- [19] J. R. Yang, C. Y. Huang, and C. S. Chiou, "Influence of plastic deformation and cooling rates on the microstructural constituents of an ultra-low carbon bainitic steel," *ISIJ International*, vol. 35, pp. 1013–1019, 1995.
- [20] S. B. Singh and H. K. D. H. Bhadeshia, "Quantitative evidence for mechanical stabilisation of bainite," *Materials Science Forum*, vol. 12, pp. 610–612, 1996.
- [21] J. R. Yang, C. Y. Huang, W. H. Hsieh, and C. S. Chiou, "Mechanical stabilization of austenite against bainitic reaction in Fe-Mn-Si-C bainitic steel," *Materials Transactions JIM*, vol. 37, pp. 579–585, 1996.
- [22] R. H. Larn and J. R. Yang, "Effect of compressive 6 deformation of austenite on bainitic ferrite transformation in Fe-Mn-Si-C steels," *Materials Science & Engineering A*, vol. 278, pp. 278–291, 2000.
- [23] T. Ko and S. A. Cottrell, "The formation of bainite," *Journal of the Iron and Steel Institute*, vol. 172, pp. 307–313, 1952.
- [24] G. R. Speich, "The growth of bainite," Ph.D. dissertation, Massachusetts Institute of Technology, Massachusetts, USA, 1958.
- [25] R. F. Hehemann, "The bainite transformation," in *Phase Transformations*, H. I. Aaronson and V. F. Zackay, Eds. Materials Park, Ohio, USA: American Society of Materials, 1970, pp. 397–432.
- [26] G. R. Srinivasan and C. M. Wayman, "The crystallography of the bainite transformation," *Acta Metallurgica*, vol. 16, pp. 621–636, 1968.
- [27] B. J. P. Sandvik, "The bainite reaction in Fe-Si-C alloys: the primary stage," *Metallurgical Transactions*, vol. 13A, pp. 777–787, 1982.

- [28] M. S. Wechsler, D. S. Lieberman, and T. A. Read, "On the theory of the formation of martensite," *Trans. AIME Journal of Metals*, vol. 197, pp. 1503–1515, 1953.
- [29] J. S. Bowles and J. K. Mackenzie, "The crystallography of martensite transformations, part I," *Acta Metallurgica*, vol. 2, pp. 129–137, 1954.
- [30] J. K. Mackenzie and J. S. Bowles, "The crystallography of martensite transformations II," *Acta Metallurgica*, vol. 2, pp. 138–147, 1954.
- [31] —, "The crystallography of martensite transformations III FCC to BCT transformations," *Acta Metallurgica*, vol. 2, pp. 224–234, 1954.
- [32] Z. G. Yang, H. S. Fang, J. J. Wang, and Y. K. Zheng, "Scanning tunnelling microscopy study of surface relief with bainite and martensite transformations," *Journal of Materials Science Letters*, vol. 15, pp. 721–723, 1996.
- [33] H. S. Fang, J. J. Wang, Z. G. Yang, C. M. Li, Y. K. Zheng, and C. X. Li, "Formation of bainite in ferrous and nonferrous alloys through sympathetic nucleation and ledge-wise growth mechanism," *Metallurgical & Materials Transactions A*, vol. 27, pp. 1535–1545, 1996.
- [34] X. Z. Bo, H. S. Fang, J. J. Wang, and Z. H. Wang, "Investigation of surface relief accompanying Widmanstätten ferrite formation by scanning tunneling microscopy," *Scripta Materialia*, vol. 39, pp. 247–252, 1998.
- [35] P. Yan and H.K.D.H. Bhadeshia, "Mechanism and kinetics of solid-state transformation in high-temperature processed linepipe steel," *Metallurgical & Materials Transactions A*, vol. DOI 10.1007/s11661-013-1907-4, p. ., 2013.
- [36] M. Peet and H. K. D. H. Bhadeshia, "Surface relief due to bainite transformation at 473 K," *Metallurgical & Materials Transactions A*, vol. 42, pp. 3344–3348, 2011.
- [37] A. Borgenstam and M. Hillert, "Bainite in the light of rapid continuous cooling information," *Metallurgical & Materials Transactions A*, vol. 27, pp. 1501–1512, 1996.
- [38] A. Borgenstam, M. Hillert, and J. °Agren, "Metallographic evidence of carbon diffusion in the growth of bainite," *Acta Materialia*, vol. 57, pp. 3242–3252, 1009.
- [39] H. K. D. H. Bhadeshia, *Geometry of Crystals*. 2nd edition, Institute of Materials, 2001.

Conclusions

- Quantitative failure analysis helps in useful recommendation and feedback as brought out in the above cited case studies:
- As a feedback to engineer, recommendation of inclusion rate for the specifications of the material for a critical component has been demonstrated.
- Quantification of microstructural degradation as a function of service exposure along with mechanical properties serves in early prevention of any catastrophic damage. As a measure of radiation damage, systematic microstructural studies help in estimation of void swelling as a function radiation dose which could play a major role in the choice of FBR core materials.
- Quantitative fractographic studies in understanding the role played by notches and determining the critical size could be a useful feedback to online monitoring assessment of defects that form serious notches.

References

- [1] Management of life cycle and ageing at nuclear power plants, Improved maintenance IAEA-TECDOC-1402, 2004
- [2] S.K.Dhua, S.K.Sen, M.S.Prasad, K.B.Mishra and S.Jha, Influence of nonmetallic inclusion characteristics on the mechanical properties of rail steel, *J Mater. Engg Perf.*, 9, p700, 2000
- [3] C. N. Venkiteswaran, V. Karthik, P. Parameswaran, N. G. Muralidharan, V. Anandaraj, S. Saroja, V. Venugopal, M. Vijayalakshmi, K. V. Kasi Viswanathan, Baldev Raj, Study of Microstructure and Property Changes in Irradiated SS316 Wrapper of Fast Breeder Test Reactor, *J ASTM International*, 6(7), p01, 2009;
- [4] J.Moteff, Effect of radiation on substructure and mechanical properties of metals and alloys, ASTM-STP 529, 1973, ASM, metals Park, Ohio, p134
- [5] R.W. Hertzberg, Deformation and Fracture Mechanics of Engineering Materials, (3rd ed), John Wiley & Sons, Singapore p 246, 1989,

Microstructure Based Design of Formable Steels

P.P. Chattopadhyay

Indian Institute of Engineering Science and Technology, Shibpur, Howrah 711103, W. B., India

Abstract

The aforesaid volume of activities is only the bird's eye view of the potential of different techniques in understanding the formation and response of microstructure in the efforts of correlating composition, process, microstructure and property in deterministic manner. It is emphasized that development of next generation high performance steel calls for interpretation microstructure in the design, rather than diagnostic paradigm. Such endeavor relies much on multiscale approach rather than the potential/limitation of the individual tool/technique. Due attention is also warranted in the efforts on integration/hybridization of the available techniques to develop the technique blends and/or multiscale combinatorial framework.

Introduction

Manufacturing of steel started in India even before the birth of Christ. Wootz steel was developed in India around 300 BC for manufacturing of the Damascus sword honed to a tough, sharp and resilient edge. In a recent report, the German scientists revealed the dispersion of nanowires of carbide encapsulated within the multiwall carbon nanotubes, in the high resolution micrograph of a blade forged from the Damascus steel. Use of woody biomass and leaves as carburizing additives along with certain specific types of iron, rich in vanadium and rare earth elements, has been attributed to the formation of the extraordinary microstructure. Worldwide manufacturing of steel continued to be based on the crucible steel technology till the beginning of seventeenth century. In 1863, Henry Clifton Sorby (10 May 1826 - 9 March 1908), for the first time, used acid etching technique to study the true microstructure of steel. Sorby's understanding, that a small but precise quantity of carbon gave steel its strength, paved the way for Henry Bessemer and Robert Forester Mushet to develop the method for mass-production of steel. In the 1890s, Adolf Martens studied the samples of different steels under microscope, and found that the hardest steels had a regular crystalline structure. He was the first to explain the cause of the widely differing mechanical properties of steels. In the 1920s Davenport and Bain discovered a new steel microstructure, which they provisionally called martensite-troostite by virtue of its occurrence

between the already known low-temperature martensite phase and what was then known as troostite (now fine-pearlite). Much latter this microstructure was named bainite by Bain's colleagues at the United States Steel Corporation.

The aforesaid understanding concerning diffusive and diffusionless transformation of austenite lead to the development of a wide range of steel with incomparable potential in different technological sectors like construction, rail, automotive, agriculture, household etc. In the course of such evolution, emergence of different varieties of alternative materials during 1980s offered fierce challenge to the steel manufacturers, particularly in transportation sector, owing to the pressing demand of weight reduction.

Since 1990s, the concerted effort by the manufacturers of automotive steel resulted into the evolution of a wide range of microstructure with an aim to maximize the strength, toughness and formability as presented in Figure 1(a). The low carbon single phase ferritic microstructures were the choice for the formability requirement while the pearlitic and Martensitic microstructure were favoured for the yield strength and UTS requirement, respectively. Extensive opportunity was exploited in terms of the variation of strength-ductility combination for a given composition of steel by controlling the thermo-mechanical process schedule with or without microalloying. The steels were generally identified in terms of the option employed for modification of the composition and/or the process schedule.

Further efforts on maximizing the conflicting properties, like strength, toughness and formability led to the development of microstructures with multiple constituent phases assigned to provide the conflicting property variables. For example, in dual phase microstructure, polygonal ferrite phase offers ductility, while martensite offers strength.

In the early 1990s, the microstructure containing bainitic phase was found to be attractive in respect of strength-ductility balance. Depending upon the presence/absence of polygonal ferrite, these microstructures were classified as ‘ferritic’ or ‘bainitic’ TRIP-aided steels. A similar class of microstructures with retained austenite as one of the key constituents was developed by subjecting the partitioning of alloying elements in austenite between martensite-start (M_s) and martensite-finish (M_f), which were identified as “Quench and Partitioning Steels”. Beside the microstructural constituents, essential feature of all such steels is the presence of varying volume fraction and carbon content of retained austenite in the final microstructure. The role of austenite and its response to strain and strain rate attracted serious attention in the endeavour of designing microstructures of TRIP-aided steels.

Recently, a class of manganese alloyed steels with fully austenite or martensite-austenite microstructures has emerged as the most potential candidate for maximization of strength-ductility-formability combination. The steels are featured by the compositionally controlled stacking fault energy which governs the onset of one or more processes of straining like slip, twinning and transformation of austenite to the ϵ or α' martensite. The futuristic design of the formable steels aims at achieving the austenite–martensite/bainite based microstructures capable to offer the enhanced combination of strength (1300-1500MPa), toughness (40,000 MPa%) and formability ($HER \approx 40-60\%$).

Microstructural evolution

In the last century, the evolution of microstructure has been manifested as the interaction between composition and process variables on the empirical framework of thermodynamic (chemistry and energy) and kinetic (time dependence) considerations. In the diagnostic framework, the potential of microstructural understanding has been

manifested as the footprint of the process and compositional attributes and blue print of the properties. Earlier, the imprecise efforts on developing the correlation among composition, process, microstructure and property were generally founded on the experimental studies, imprecise “if-then” knowledge and fewer empirical correlations. Gradually, the constitutive relationships were invoked in the understanding thermodynamic and kinetic aspects of the phase evolution. e.g., austenite recrystallization [1], austenite to ferrite transformation [2] as well as low temperature transformation behavior of austenite to martensite [3] or bainite [4]. The contemporary understanding of microstructure in the design framework is depicted in Figure 1(b).

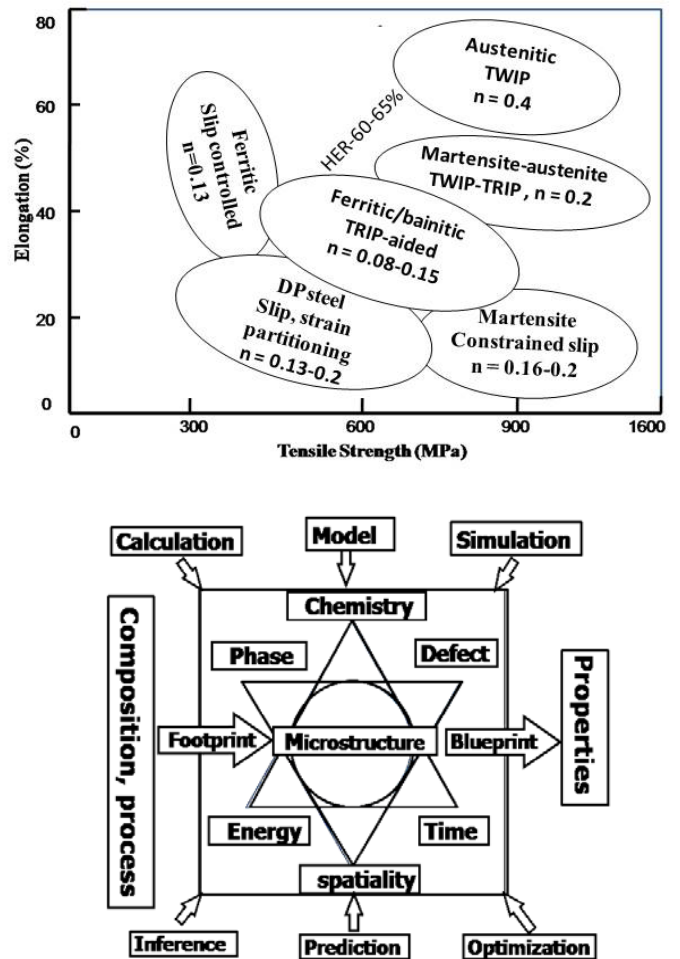


Figure 1. (a) microstructure based performance mapping (b) framework of microstructure based design.

Modeling and simulation of microstructure

Atomistic/microscale techniques

During last couple of decades the availability powerful computers has empowered the scientific community to deal with the numerical complexity of realistic problems in deterministic manner. Great deal of efforts has been devoted in understanding of the atomic scale behavior of materials and to employ the understanding in multiscale framework. Such *Ab initio* approaches are based on the parameter-free, fundamentally, quantum-mechanical description of a system as made of interacting electrons in the field of atomic nuclei (first principles calculations). The reasons for this success lie in the original reformulation of the many-particle Schrödinger equation (Density Functional Theory) coupled with physical insight for the correlation effects of the interacting electrons (Local Density Approximation).

Recent progress in methods based on density functional theory (DFT), now makes possible the exploration of chemical trends, the determination of parameters for phenomenological models and the identification of new routes for the optimization of steel properties. The approach combines electronic, vibrational and magnetic effects as well as structural defects in an integrated framework. The simulation tools allow predicting the mechanical and thermodynamic properties of metals with high level of accuracy. Application of DFT based approach in steel design has been comprehensively reviewed by Hickel *et al.* [5].

Molecular dynamic (MD) simulation considers that atom in a N-body system obey the classical Newton law through the potential energy. MD simulation has been found successful as a typical microstructural simulation tool for capturing the atomic scale material behaviour and the statistical properties of the macro materials. In steel research, the simulation tool has been employed to study the hitherto inaccessible phenomena like effect of C on the nucleation of stacking fault [6]. In an attempt of multiscale simulation of the TRIP-aided behaviour, the microscale MD simulation has been successfully coupled with macroscale finite element simulation [7].

Some numerical simulations have described the transformation kinetics depending upon the finite mobility of the moving interface and diffusion of carbon in binary Fe-C alloys [8-9]. The crucial assumption in such physically based models is that the chemical potential of interstitial components of both sides of sharp interface has to be equal, so that there is no trans-interface diffusion of carbon. De Meyer *et al.* [10] obtained the distribution of C, Mn and Si at ferrite-austenite boundary by using local equilibrium model calculation at 810°C. The carbon content of the intercritical austenite has been calculated by taking into account the influence of Si, Mn and Al.

Meso-/macro-scale techniques

The aforesaid models essentially deal with the phenomena considering the average state of the microstructure. However, realistic description of the structure-property correlation necessitates the prediction of the morphology of the grains and to follow the nucleation and growth of the individual grains and their mutual interaction.

The microstructural simulation models concerning the kinetics of the evolution may be broadly classified into two categories, Firstly sharp interface models and secondly diffused interface models as depicted in Figure 2 [11].

Cellular Automaton (CA) and Monte Carlo-Potts (MC) technique are considered in the category of sharp interface techniques. Formally, CA is an array of the finite-state machines in one, two or three dimensions, governed by rules of changing the state of cells in the array. In order to CA to operate, two sets of rules are required to be specified: i) the extent of the interaction between the cells in the array and ii) the transition of the cells. A simple example of the CA can be set up by arranging number of coins on a table in a line or square grid. If the coins are placed in randomly on the table, some will fall head while others be tail. In CA, the rules need to be invented by which coins is turn over. In steel research CA has been primarily applied to the simulate solidification [12-13], static [14] and dynamic [15] recrystallization during hot working, static recrystallization in cold worked interstitial free steel [16], and austenite-ferrite transformation [17].

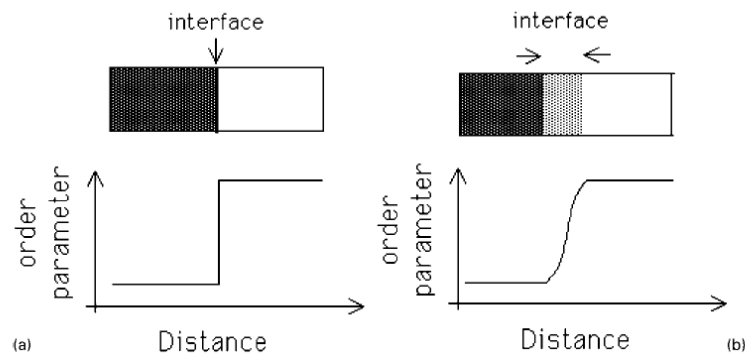


Figure 2. (a) Sharp interface approach and (b) diffused interface approach [11]

Monte Carlo technique refers to any method that utilizes sequences of random numbers to perform statistical simulation. The main requirement to use Monte Carlo method for simulation of a physical system is that it must be possible to describe the system in terms of probability density function (PDF), also called partition function (Z). Once the PDF or Z for a system is known, then the simulation begins by random “sampling” from the PDF, and subsequently determining the desired properties of the sample by conducting some kind of a “trial”. In contrast to CA, where cells at the centre of simulation need to be tagged as such, and their neighborhood need not to be inspected and calculation are only required at the boundary of a growing grain or second phase, the basic MC approach selects the sites at random from the lattice of calculation points without reference to the microstructure that is being considered. Thus as the grains grows or transformation proceeds, the calculation points increases leading more calculation per time step. MC has been identified as a potential simulation tool to study grain growth under the influence of second phase [18], Goss texture development in silicon steel in the presence of MnS particles [19], isothermal austenite–ferrite transformation under non-equilibrium interface condition [20], and austenite–ferrite diffusive transformation during continuous cooling [21].

The phase field simulation is basically a meso-scale simulation technique, based on the diffused

interface approach, considering a number of grains. The shape and mutual distributions of the grains are represented by set of field variables, which are continuous in space and time [22]. Within the grains, the values of phase field variables are constant, while at the interface between the two grains the phase field variables gradually vary between their values in neighboring grains. These phase field variables may be conserved or non-conserved depending upon relation to local composition and local crystal structure orientation respectively. The equation for the evolution of phase field variables are derived on the basis of the chemical thermodynamic and kinetic information available from tools like MTDATA [23], ThermoCalc [24–26], Dictra [27] etc.. However, they don’t deal with the behavior of individual atoms, so material properties must be introduced in the model through phenomenological parameters that are determined on the basis of the experimental and theoretical information. In steel research, phase field simulations has been applied to the wide variety of applications including the solidification [28–29], diffusive [30–33], and non-diffusive transformations [34–37]

In view of the above, a scheme for determination of austenite grain size evolution during hot rolling by using the combination of different techniques is schematically depicted in Figure 3.

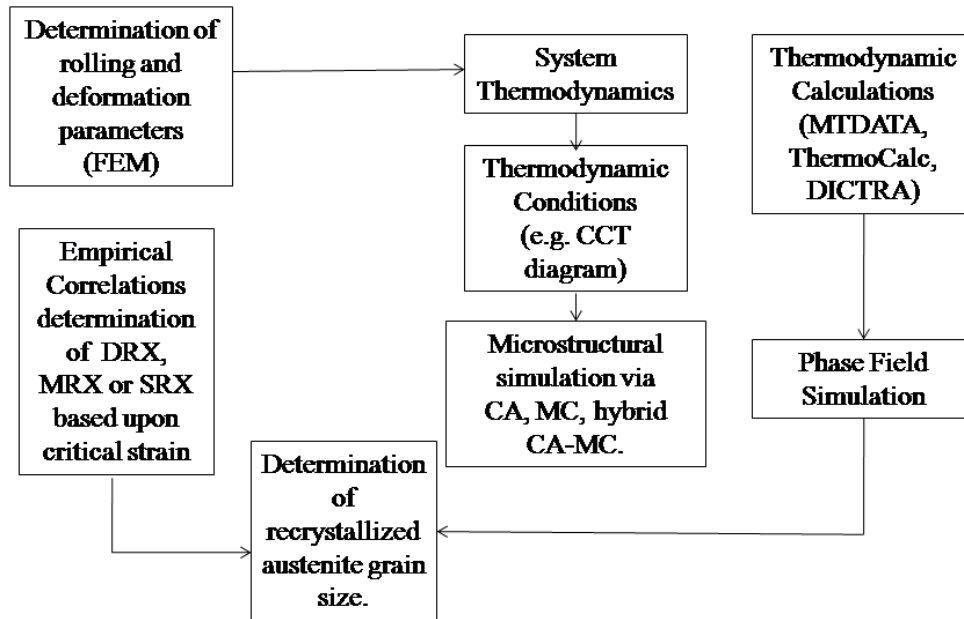


Figure 3. Model for phase transformation during cooling and coiling in hot-strip mill

Microstructure-property correlation

Microstructure-property correlation has been modeled by involving the mechanistic parameters. The stress strain behavior of single phase microstructure may be approximated by Mecking-Kocks model [38-39], where the evolution of dislocation density depends upon the competitive hardening and softening. In contrast, the deformation behavior of the dual phase steel is typically defined by the composite model consisting of hard and soft phase. Mileiko model [40] has been successfully used to obtain the deformation parameters of the dual phase steels. Successive application of mixture law on the independent behavior of constituent phases has been used to describe the stress-strain behavior of multiphase TRIP-aided steels [41] as depicted in Figure 4. The stress-strain behavior of the individual constituent phase is determined by considering the Mecking-Kocks model. The role of twinning in strain hardening was proposed by Remy [42], considering the twin spacing to mean free distance of the dislocation. The other approach of modeling concerns the dynamic reduction of the mean free

path of dislocation by the twin boundary [43-44]. It also considers the Mecking-Kocks theory to relate the evolution of the statistically stored dislocation and isotropic hardening behavior of the material.

Soft computing approach

Knowledge based design of microstructural evolution governed by complex correlation are often constrained by the inaccessibility of certain mechanisms, concerning the interactions among the composition and process parameters, by experimental techniques or physical modeling. In such cases data driven models have been designed to capture the complexity of the problem among the variables on the basis of available information and rules in global scale. In recent times, a group of data/rule driven soft computing techniques have been employed in the efforts of composition-process-microstructure-property correlation of steel based on the available information and imprecise knowledge. The popular soft computing techniques are Fuzzy inference system (FIS), Artificial neural network (ANN) and Genetic Algorithm (GA) which find useful application in steel research[45].

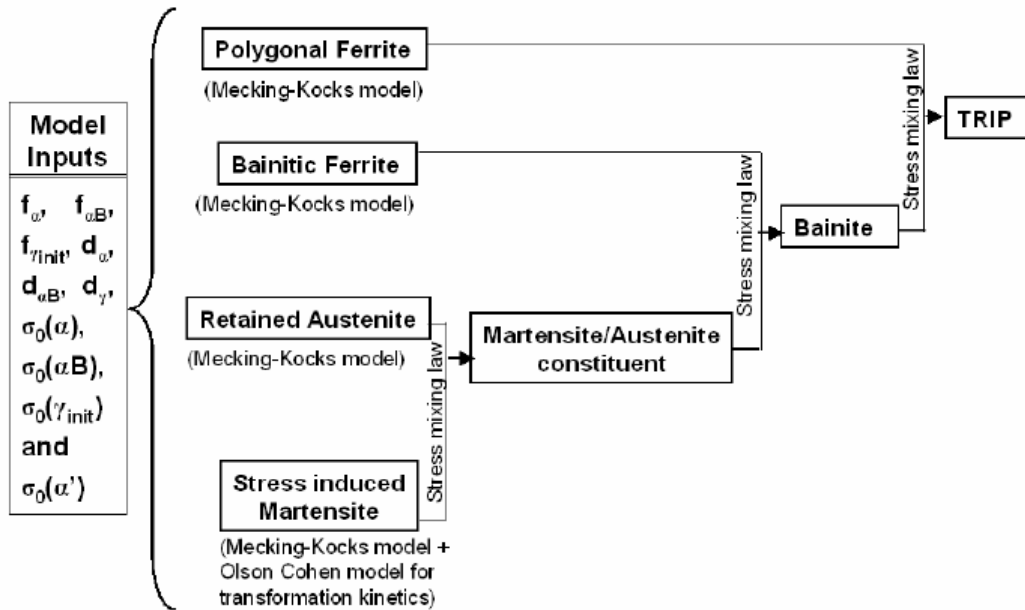


Figure 4. Decomposition of multiphase TRIP steel and application of Mecking-Kocks model and Stress mixture law for determination of stress-strain curve.

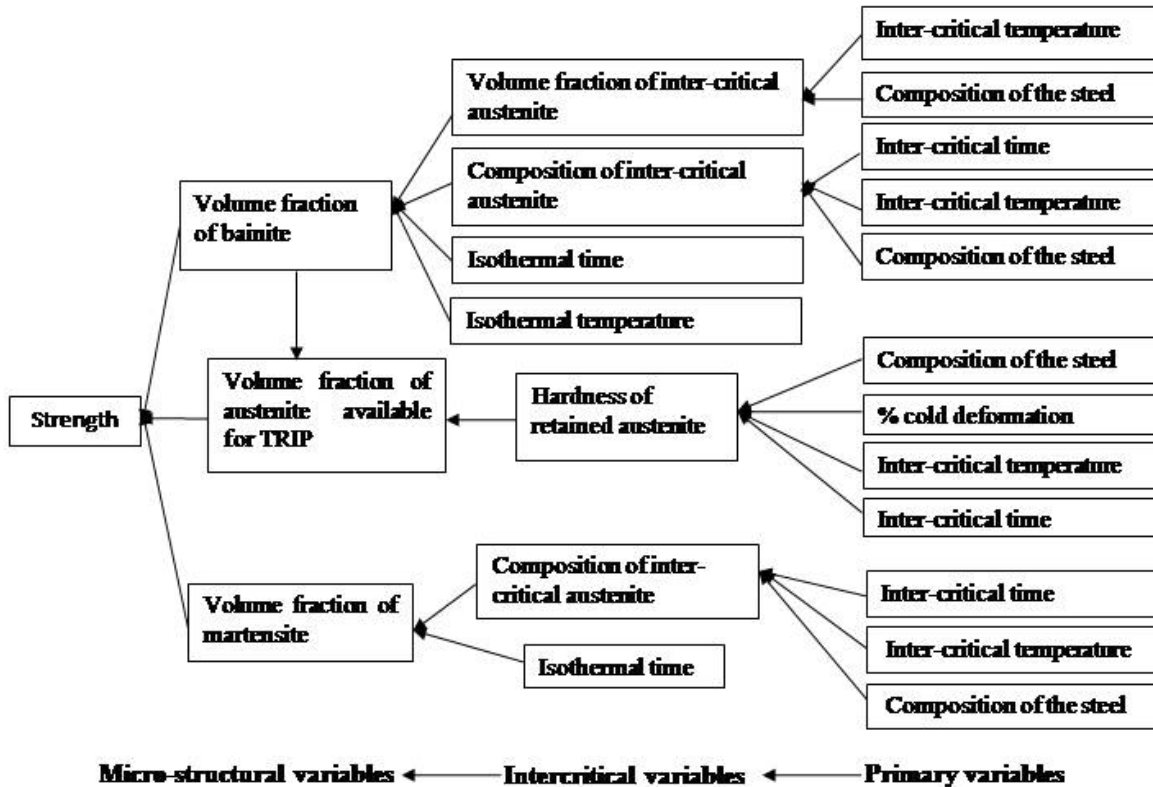


Figure 5. Sequential correlation of composition process microstructure and property for TRIP-aided steel [46].

Fuzzy inference system

Figure 5 elaborates the hierarchical connectivity of the variables those contribute in evolving the microstructure and mechanical properties of the TRIP-aided steels. In the imprecise knowledge based approach the parameters at each layer are quantitatively evaluated with some membership (e.g., high, low, medium etc.) and the parameters are connected by some linguistic rule. For example: IF (C in steel is *medium* and Intercritical temperature is *low* THEN austenite volume fraction is *low* and carbon content of austenite is *high*). Here *low*, *medium* and *high* carry some membership value. The membership value (or degree of membership) of each point in the input space, called Fuzzy value, is mapped to a value between 0 and 1 by a membership function (MF). Fuzzy linguistic descriptions through fuzzy IF-THEN rules are formal representations of system knowledge as furnished below:

IF (x is A , y is B , ...) THEN (p is M , q is N ...)

Here, the linguistic variables x and y take the values of fuzzy sets A and B , respectively. The IF-THEN rule combines the membership based on the rule strength and results into the fuzzy output as p and q for the output variables M and N , respectively.

Based on the Fuzzy framework, an attempt has been made to estimate the strength of TRIP-aided steels. It is evident from Figure 5 that the first, second and third layers comprise the variables concerning composition /process, intercritical and macrostructural parameters, respectively. In the framework, variables in each layer have been derived from the preceding layer through the Fuzzy

rules. Finally, the strength is derived from the variables in the third layer. Figure 6 presents the comparison of the target and achieved strength values for different steels. The comparison demonstrates that even in the absence of any constitutive correlation a reasonable agreement has been achieved keeping the inherent complexity and nonlinearity of the system in view [46].

Artificial neural network

An ANN model consists of a set of interconnected computing units called neurons which interact with each other through connection strength, called weights. In the training process of the network, the difference in the target and prediction, i.e., the error is back propagated in the network and the connection weights are adjusted accordingly to get a better response. Finally, the trained network is employed for prediction of the output against the given set of input values chosen within the range of values assigned for the variables. The ANN technique has been elegantly implemented in prediction CCT diagrams. For this purpose, the available CCT diagrams in the literatures have been suitably digitised to develop the numerical dataset comprising the start and finish time and temperatures for different phases at a given cooling rate. The dataset has been utilised for training the network and subsequently employed for prediction of the CCT diagrams. It is apparent from figure 7 that the predicted diagram compares well with the actual diagram [47].

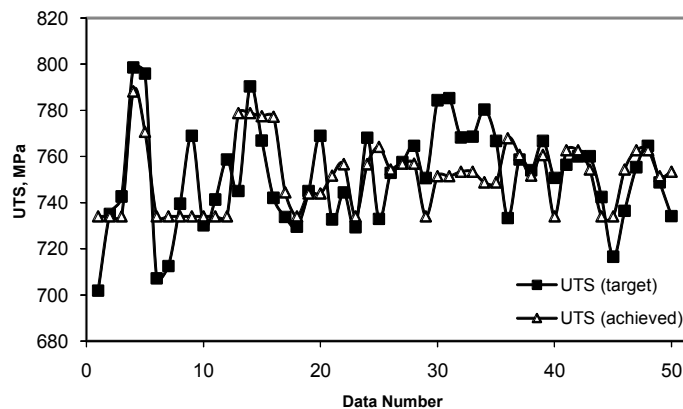


Figure 6. Comparison of target and achieved properties for the fuzzy based model of TRIP-aided steel [46].

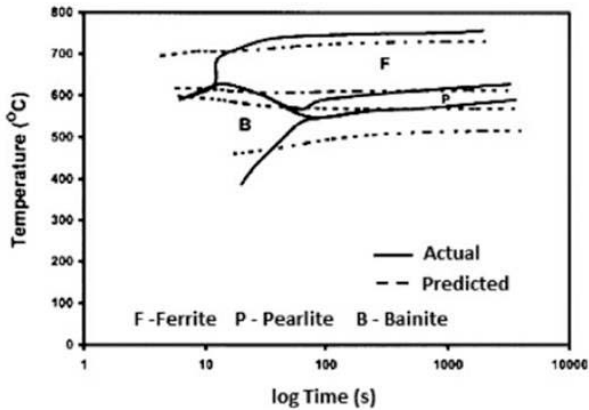


Figure 7. Comparison of the actual CCT diagram with the same predicted by the ANN model [47].

Genetic algorithm

Genetic algorithm (GA), is a evolutionary algorithm based stochastic global search method capable to mimic the principles of natural selection and natural genetics [72] to find the best solution for a specific problem. GA operates on a population of feasible solutions to produce better approximations to a solution applying the principle of survival of the fittest. The solutions are upgraded through crossover and mutation in each successive generation till the desired fitness is achieved or the predetermined number of generation is completed.

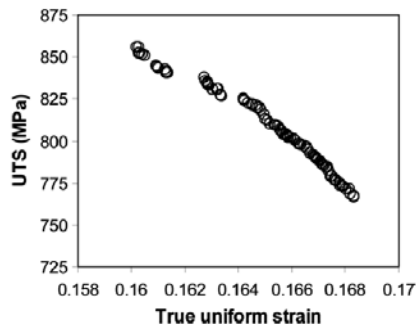


Figure 8. Pareto front obtained from GA-based optimisation for TRIP-aided steel [48].

In an attempt to optimize the strength and elongation of TRIP-aided steels, GA has been employed using the model presented in Figure 4 as the objective function [48]. The profile of the non-dominated solutions obtained at the end of the target number of generations, known as pareto front, is presented in Figure 8. The essence of non dominated solution is that there exists no other solution which is a better solution in the solution space.

Micromechanical modeling

The mechanical performance of steel grades depends strongly on the microstructure. Important parameters are: spatial distribution of the phases, volume fractions, size and shape distributions of particles and grains. Standard voronoi tessellations are widely used for this purpose and powerful in creating different complex patterns. By applying different generating point fields (random Poisson, distorted grid, centre of mass, clustered, hard core etc) a wide range of microstructures can be created. In an effort to develop different microstructure of dual phase (DP) steel, Kok et al, have proposed a scheme for development of multilevel Voronoi structure [49]. At the first level a point field is used to create a fine tessellation of Voronoi cells. After that a second level coarser tessellation is created with another less dense point field. This serves as a master for the construction of complex shaped grains. Thus, in the multilevel Voronoi structure, the finer and coarser tessellations represent the martensite phase and ferrite grain, respectively. By modifying point field densities of both levels the user is able to generate a broad range of different shapes and sized grains [50].

To elucidate the deformation behavior of the microstructure, the representative volume element (RVE) is assumed to deform under generalized plane strain loading condition. With an aim to estimate the stress and strain distribution in the microstructure in the course of plastic straining, a micro-mechanical model has been developed and analyzed using the finite element program ANSYS. In order to simulate the uniaxial loading condition, the boundary conditions were applied at extreme ends. Both the phases of DP steel were modeled as the isotropic continua, the Von Mises criterion being used to calculate the onset of the plastic deformation in each phase. The details of the analyses are reported elsewhere [50]. Figure 9 exemplifies the variation of microstructures in terms of the martensite (dark constituent) size shape and the corresponding distribution of equivalent plastic strain. It is apparent from the figure that the strain is concentrated more in the locations of banding and/or higher martensite connectivity. By using the variation of strain concentration data for varying microstructures a correlation has been developed between area of maximum strain concentration and contiguity parameters among the phases by employing the genetic programming (GP). The correlation is expressed by the following equation:

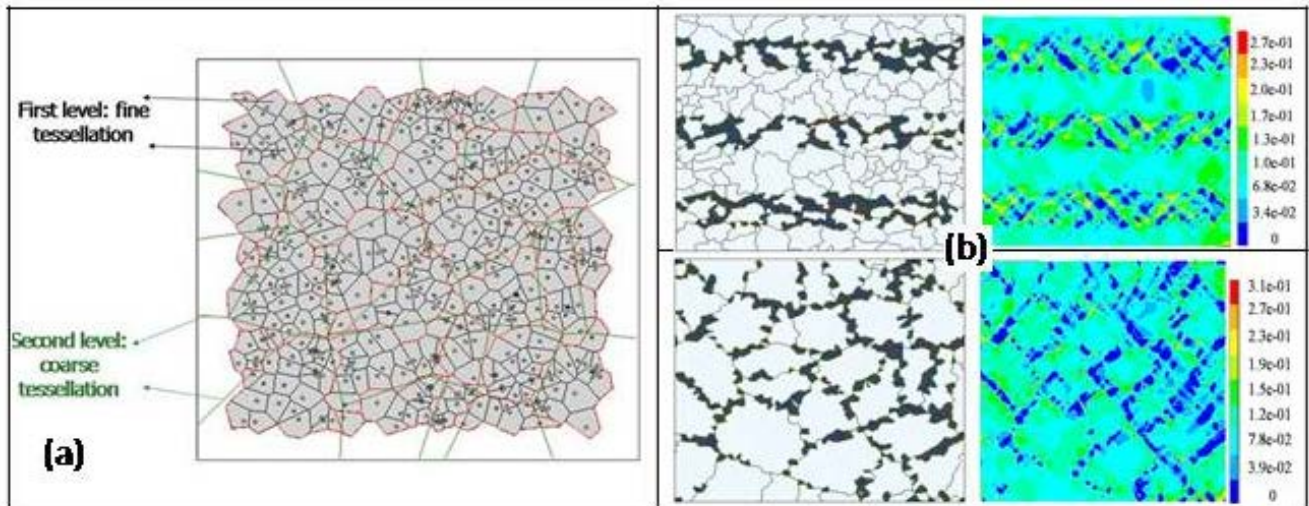


Figure 9. Shows (a) the scheme for development of the multilevel Voronoi structure and (b) the simulated microstructures and corresponding distribution of the equivalent strain.

$y = 4.1935 + 0.1566 * \{(MCP - 0.4457) / (0.5936 - FCP)\}$
 where y is strain and MCP and HCP are the martensite and ferrite contiguity parameters, respectively.

Summary:

The aforesaid volume of activities is only the *bird's eye view* of the potential of different techniques in understanding the formation and response of microstructure in the efforts of correlating composition, process, microstructure and property in deterministic manner. It is emphasized that development of next generation high performance steel calls for interpretation microstructure in the design, rather than diagnostic paradigm. Such endeavor relies much on multiscale approach rather than the potential/limitation of the individual tool/technique. Due attention is also warranted in the efforts on integration/hybridization of the available techniques to develop the technique blends and/or multiscale combinatorial framework.

Reference

- [1] X. Li, M. Wang, F. Dua, Materials Science and Engineering A, 408 (2005)33.
- [2] E. Gamsjager, F. D. Fisher and J. Svoboda, Mater. Sci. Tech., 125(2004)959.
- [3] J. Wang and S. Van der Zwaag, Metall. Trans., 32(2001)1527.
- [4] H. K. D. H. Bhadeshia. Bainite in Steels. IOM Communications Ltd, London, second edition, 2001.
- [5] T Hickel, B Grabowski, F Kormann and J Neugebauer, J. Phys.: Condens. Matter 24 (2012) 053202.
- [6] H. Y. Li, X. Ch. Li, J. H. Li, J. L. Ma, Y. J. Zhang, Adv. Mater. Res., 827(2014) 8.
- [7] H. Y. Li, X. Ch. Li, J. L. Ma, J. H. Li, Y. J. Zhang, Appl. Mech. and Mater., 423-426(2014)182.
- [8] G.P. Krielaart, J. Sietsma, S. van der Zwaag, Material Science and Engineering A, 237(1997) 216.
- [9] J. Svoboda, F. D. Fisher, P. Fratzal, E. Gamsjager and N. K. Simha, Acta Mat., 49(2001) 1249.
- [10] M. De Meyer, J. Mahieu and B.C. De Coomen, Mater. Sci. Tech., 18(2002)1121.
- [11] X. Liang, J. R. McDermid, O. Bouziz, X. Wang, J. D. Embury and H. S. Zurob, Acta Mater., 57(13)(2009) 3978.
- [12] M. Rappaz and C. A. Gandin, Acta Metallurgica and Materialia, 41(1993)345.

- [13] J. A. Spittle and S. G. R. Brown, *Acta Metallurgica and Materialia*, 42(1994)1811.
- [14] S. Das, E. J. Palmiere, and I. C. Howard, *Materials Science Forum*, 623(2004)467.
- [15] M. Qian and Z. X. Guo, *Materials Science and Engineering A.*, 365(2004)180.
- [16] D. Raabe and L. Hantcherli, *Computational Material Science*, 34(2005) 299.
- [17] M. Tong, D. Li, and Y. Li, *Acta Materialia*, 52(2004)1155.
- [18] C. Ming Huang, C.L. Joanne, B.S.V. Patnaik, R. Jayaganthan, *Appl. Surf. Sci.*, 252 (2006) 3997.
- [19] N. Rajmohan, J.A. Szpunar, *Mater. Sci. and Eng. A* 289 (2000) 99.
- [20] Mingming Tong *, Dianzhong Li, Yiyi Li, *Acta Materialia* 53 (2005) 1485.
- [21] Mingming Tong *, Dianzhong Li, Yiyi Li, *Acta Materialia* 52 (2004) 1155.
- [22] R. Qin and H. K. D. H. Bhadeshia, *Mater. Sci. Tech.*, 26(7)(2010)803.
- [23] R. H. Davies, A. T. Dinsdale, J. A. Gisby, J. A. J. Robinson, S. M. Martin, *CALPHAD*, 26(2)(2002) 229.
- [24] M. Hillert, *Phase Equilibria Phase Diagrams and Phase Transformations*, (1999) Cambridge Univ. Press, ISBN 0-521-56270-8.
- [25] B. Sundman, B. Jansson and J-O. Andersson, *CALPHAD*, 9 (1985) 153.
- [26] B. Sundman, *Anales de Fisica, Serie B*, 86 (1990) 69.
- [27] J. O. Anderson, T. Helander, L. Hoglund, P. Shi and B. Sundman, *CALPHAD*, 26(2) (2002)273.
- [28] J. Tiaden, *J Cryst Growth*, 198-199(1999)1275.
- [29] J. Li, N. Provatas, *Metall Mater Trans B*, 39(2008)268.
- [30] G. Pariser, P. Shaffnit, I. Steinbach, W. Bleck, *Steel Res.*, 72(2001) 354.
- [31] I. Loginova, J. Ågren, G. Amberg, *Acta Mater*, 52(2004) 4055.
- [32] Matthias Militzer, *Current Opinion in Solid State and Materials Science*, 15(2011) 106
- [33] A. Yamanaka, T. Takaki, Y. Tomita, *Mater Sci Eng A*, 480(2008) 244.
- [34] A. Artemev, Y. Jin, A. G. Khachaturyan, *Acta Mater*, 49(2001)1165.
- [35] O. U. Salman, A. Finel, R. Delville and D. Schryvers, *J. Appl. Phys.*, 111(2012)103517.
- [36] Hemantha Kumar Yeddu, Annika Borgenstam, Peter Hedström, John Agren, *Materials Science and Engineering A*, 538(2012)173.
- [37] J. Kundina, D. Raabe, H. Emmerich, *Journal of the Mechanics and Physics of Solids*, 59(2011) 2082.
- [38] B. P. J. Sandvik and H. P. Nevalainen. *Metal. Tech.*, June(1981)213.
- [39] S. Curtze and V. T. Kuokkala, *Acta Mater.*, 58(2010)5129.
- [40] S. T. Mileiko, *J. Mater. Sci.*, 4(1969)974.
- [41] J. Bouquerel, K. Verbeken and B.C. De Coomen, *Acta Mater.*, 54(2006)1443.
- [42] L. Rémy, *Acta Metall*, Vol. 26, 1978, pp 443.
- [43] I. Karaman, H. Sehitoglu, A. J. Boudin, Y. I. Chumlyakov, H. J. Maier and C. N. Tome, *Acta Mater.*, 48(2000) 2031.
- [44] O. Bouaziz, N. Guelton, *Mater Sci Eng A*, 246(2001) 319.
- [45] S. Datta and P. P. Chattopadhyay, *International Materials Reviews*, 58(8) 2013(475).
- [46] S. K. Ghosh, P. P. Chattopadhyay, A. Haldar, S. Ganguly and S. Datta: *ISIJ Int.*, 48(2008)649.
- [47] S. Dey, S. Datta, P. P. Chattopadhyay and J. Sil: *Comput. Mater. Sci.*, 43(2008) 501–511.
- [48] S. Ganguly, S. Datta, P. P. Chattopadhyay, and N. Chakraborti, *Materials and Manufacturing Processes*, 24(2009) 31.
- [49] S. Yadegari, S. Turteltaub, A. S. J. Suiker, P. J. J. Kok, *Comp. Mater. Sci.*, 84(2014) 349.
- [50] G. Anand, P. Dey, P. J. J. Kok, D. Chakraborty, and P. P. Chattopadhyay, *Materials Science and Technology*, 2014, DOI 10.1179/1743284714Y.0000000535.

Quasicrystal: Bulk to Nano

T.P. Yadav^{1*}, N.K. Mukhopadhyay² and O.N. Srivastava¹

1. Hydrogen Energy Centre, Department of Physics, Banaras Hindu University, Varanasi-221005, India

2. Department of Metallurgical Engineering, Indian Institute of Technology (BHU), Varanasi-221005, India

*Corresponding authors: E-mail: yadavtp@gmail.com, Phone: +91 542 2307307, Fax: +91 542 238468

Abstract

Quasicrystals are of great interest because of their extraordinary physical properties and applications such as catalytic agent, hydrogen storage materials, photonics materials. The quasicrystal-composites can be fabricated through various routes. In this review, we discuss the basics of quasicrystal synthesis both in bulk and nano forms.

Keywords. Quasicrystal, Icosahedral phase, Decagonal phase, Nano-materials; High energy ball milling

Introduction

Before the discovery of quasicrystals, atomic structures of solids are conventionally divided into two classes. These are crystalline and glassy structures. Crystal structures are characterized by translational periodicity and rotational symmetry. Interplay of the two imposes restrictions on each resulting in the 14 three dimensional Bravais Lattices and the 32 point group having only 1,2,3,4, and 6 fold rotational symmetry axes. These requirements also ensure bond orientational order in crystals. A glassy structure in contrast has neither long range translational nor bond-orientational orders. Such structures are usually modeled by a dense random packing of spheres.

In 1984, Shechtman, Blech, Gratias and Cohn reported the existence of a phase in a rapidly solidified Al-14% Mn alloy that exhibited diffracted patterns consisting of sharp Bragg peaks and had icosahedral point group symmetry (m35) [1]. Icosahedral symmetry displaying five-fold rotation axis, is incompatible with translational symmetry. However sharpness of the spot indicates long range order. This paradox was soon resolved by constructing a quasi periodic structure with an icosahedral bond orientational order which showed diffraction patterns almost exactly similar to the observed ones. The observed phase has now been

identified to have a new class of ordered structure with a perfect icosahedral bond orientational and a quasi periodic translational orders. They have thus been called quasiperiodic crystals or more commonly a quasicrystal. We can state that quasicrystal are material with perfect long-range quasiperiodic order but with no three dimensional translational periodicity. The former is manifested in the occurrence of sharp-diffraction spots, and the latter conforms to non-crystallographic rotational symmetry. Since then many stable and metastable quasicrystals were found.

Synthesis of quasicrystalline materials

Initially the icosahedral quasicrystal was reported by Shechtman et al (1984) to occur in Al-14% Mn alloy by the melt spinning technique [1]. Later on, a variety of methods has been developed to synthesize the quasicrystalline phases. These techniques include: (i) Rapid solidification from the melt [1], (ii) Air atomization [2], (iii) Rapid pressurization of the melt [3], (iv) Chill casting [4], (v) Directed energy processes [5-7], (vi) Devitrification of metallic glasses [8], (vii) Precipitation from supersaturated solid solutions [9-10], (viii) Mechanical alloying/milling [11-14], (ix) Gas evaporation [15].

The rapid solidification technique mainly employs melt spinning and twin roller quenching of

molten metal onto fast rotating sinks. To study the nucleation and growth process of quasicrystals, laser or electron beam processing technique is useful as it gives a wide range of cooling rates depending upon the scanning rate and high under cooling due to substrate quenching. Electrohydrodynamic atomization technique has also been employed to rapidly solidify micron and submicron size droplets to understand the nucleation behaviour of quasicrystals. A novel solidification technique namely rapid pressurization has been used to produce quasicrystalline alloy. In this method a molten alloy is rapidly pressurized to in ≤ 20 ms in a simple piston cylinder apparatus. In casting method millimeter sized quasicrystals have been obtained which is very useful for physical properties measurements. The directed energy processes have been found to produce the icosahedral phase in vacuum deposited multilayer quasicrystalline thin films. In this case, the icosahedral phase has either been obtained by the mixing of the Al/Mn layers of ion beams or electron beam or by thermal annealing of ion beam amorphized Al/Mn thin films [5-7]. It has been found possible to obtain the icosahedral phase by thermally assisted interdiffusion of vapour deposited Al/Mn layers in the solid state. The quasicrystals produced by these methods are of very fine size. In a rapidly solidification, amorphous to icosahedral phase transformations have been investigated.

Stability of Quasicrystals

The stability of quasicrystals is of interest. All metastable quasicrystals are easily transformed to into some crystalline phase under suitable conditions but the stable quasicrystals are stable up to the melting temperature. The conventional thinking about the possibility of 5-fold symmetry and the necessity of crystallographic point-group symmetry as a must for the stability of long range atom order, the metastable nature of the quasicrystalline phases were first thought to be imperative. It is known that QC phase undergoes a structural transformation to various types of crystalline phases during annealing [16], ion milling [17], electron beam irradiation [18], mechanical testing [19] and mechanical milling [20-22]. Many thermally stable quasicrystalline materials have been discovered. Since then extensive work has been carried out to understand

the formation, phase stability and structure of this phase in order to exploit it for possible industrial applications. Therefore the first report of the occurrence of stable quasicrystalline phase in Al_6CuLi_3 alloys came as a surprise [23]. This discovery of stable quasicrystal system was further in forced by the occurrence of several other new stable quasicrystal phase in alloy system like Al-Cu-Fe and Al-Cu-Ru, Ag-In-Yb [24-26]. These stable quasicrystal systems were to face centered icosahedral type. Occurrence of stable decagonal phase like Al-Cu-Co and Al-Co-Ni has also been reported [27-28].

The stability of these quasicrystalline alloy systems were accounted for Hume-Rothery type of phase stabilization. According to the Hume-Rothery criterion stability of given alloy depends upon its total free electron concentration (i.e. the e/a ratio). Depending upon the electronic bond structure of the alloy there would be a minimum in the density of state. For a given alloy (i.e. for a specific value of e/a) the phase for which Fermi level (E_f) lies at minimum, the density of state would be stable. The minimum in the causes of the lowering of electronic energy and hence the stabilization of the phases. The theory of the construction of Brillouin Zone (BZ) accounts that at the zone boundary the density of state is zero, and depending upon scattering efficiency a gap may also appear. This implies that the phase for which the E_f lies vicinity of the Brillouin Zone boundary or when the Fermi surface touches (or interact) the BZ boundary, that would be stable. By the general free- electron consideration (considering the valence electron per atom) it has been shown qualitatively that the free electron Fermi wave vector $k_f \approx Q/2$ (where $Q=2/d$) where Q is the reciprocal lattice vector corresponding to the most intense diffraction spot. In this case of reciprocal quasicrystal due to the large degeneracy of the reciprocal lattice vectors the shape of the corresponding pseudo Jones-Zone boundary is nearly spherical giving rise to a Fermi surface Jones Zone bounding interaction and hence the lowering of the electronic energy and the stabilization of the phase. The criterion $K_f = Q/2$ have been found to follow in several quasicrystalline alloy systems. This criterion indicates that the change in composition may bring the E_f in exact contact, with the pseudo Jones Zone giving raise the stabilization against thermal treatment. In fact this has been found to occur in several alloy systems [29-30].

Properties of quasicrystals

(i) Mechanical properties and deformation behavior

Like many intermetallics, quasicrystals are hard and brittle at room temperature, partially because of their nonperiodic atomic structure [31]. Quasicrystals also show a low surface friction and high wear resistance. A single icosahedral $\text{Al}_{70}\text{Pd}_{10}\text{Mn}_{20}$ quasicrystal (51) prepared by the Czochralski method has a high Young's modulus of 200 GPa and a high Vickers hardness of approximately 750 at room temperature, although the quasicrystal is extremely brittle [32]. However, like many intermetallics, quasicrystals can be ductile at high temperatures above 0.6 – 0.8 T_{mand} and exhibit work softening [33]. The concept of dislocation in quasicrystal has been established [34]. Deformation experiments at high temperatures were performed for a polygrained icosahedral quasicrystalline Al-Cu-Ru sample [35]. Later, direct evidence of deformation by a dislocation mechanism was revealed. Dislocation glide was also directly observed in in-situ deformation experiments in a transmission electron microscope [36]. The dislocation motion has been investigated by computer simulation in a decagonal quasicrystal and an icosahedral quasicrystal [37]. High-temperature deformation experiments have been performed for icosahedral Al-Cu-Fe and Al-Pd-Mn samples. Hardness for Al-Pd-Mn gradually decreases up to approximately 600 K but, at greater than 600 K, changes its slope and decreases rapidly, suggesting that the deformation mechanism changes at approximately 600 K. A possible mechanism of work softening in the case of the dislocation motion is controlled by the Peierls mechanism [38]. Cluster friction is another possible mechanism controlling dislocation motion [39].

(ii) Electrical properties

Partially because quasicrystals lack translational periodicity, they possess high values of electrical resistivity approximately 100–300 m Ω cm at room temperature [40], and many of them have a negative coefficient of temperature dependence. The resistivity of quasicrystals is large compared with that of crystalline intermetallics at low temperature

and decreases with increasing temperature. Quasicrystals' temperature dependence of conductivity is qualitatively similar to that of various disordered systems undergoing a metal-insulator transition, such as amorphous metal-semiconductor alloys. However, such behavior is also observed for metallic quasicrystals. Some simulations using approximants indicate the existence of a pseudogap around the Fermi energy [41]. In particular, the electrical resistivity, magnetoresistance, and specific heat of the binary icosahedral $\text{Cd}_{5.7}\text{Yb}$ quasicrystal and an approximant, Cd_6Yb , were measured [42]. The icosahedral phase and the approximant showed a large positive temperature coefficient of the resistivity at less than 200–300 K. A stepwise change of the resistivity of an approximant at 110 K occurred. Giant magnetoresistance of 200% at 9 T was observed for the icosahedral phase at less than 4.2 K. The value of the electronic specific heat coefficient ' γ ' is also large for the icosahedral phase and for the approximant. Furthermore, the Debye temperatures are 142 K and 144 K for the icosahedral phase and approximant, respectively. Electrical properties of the polyquasicrystalline icosahedral $\text{Al}_{72}\text{Pd}_{19.5}\text{Mn}_{8.5}$ phase were studied in the temperature range of 10–300 K [43]. A single $\text{Al}_{64}\text{Cu}_{23}\text{Fe}_{13}$ quasicrystal shows an electrical resistivity of 3950 $\mu\Omega$ cm and a negative temperature coefficient [44]. However, the maximum value of the electrical resistivity of a $\text{Zn}_{60}\text{Mg}_{30}\text{Ho}_{10}$ alloy of 159 $\mu\Omega$ cm is comparatively lower than other quasicrystal systems [45]. According to their relatively low electrical conductivity, quasicrystals are also quite poor thermal conductors because these two properties of metals and alloys are connected.

(iii) Magnetic properties

Typical quasicrystals show either weak paramagnetic or diamagnetic properties. For example, the magnetic properties of an icosahedral Cd-Mg-Tb quasicrystal [46] and an icosahedral R-Mg-Zn quasicrystal were studied Where $R = \text{Y}$, $(\text{Y}_{1-x}\text{Gd}_x)$, $(\text{Y}_{1-x}\text{Tb}_x)$, Tb, Dy, Ho, and Er [47]. The magnetic susceptibility of Zn-Mg-R icosahedral quasicrystals obeys the Curie-Weiss law at high temperatures. The magnetic properties of

Zn₆₀Mg₃₀Ho₁₀ were investigated in the temperature range between 2 K and room temperature [46]. At less than 15 K, the magnetic-field dependence exhibited a maximum of magneto resistance. The temperature dependence of the magnetic susceptibility followed the Curie-Weiss law between 10 K and room temperature. At less than freezing temperature T_f , some quasicrystals containing RE elements exhibited a large difference between field-cooled and zero-field-cooled magnetic susceptibilities [47-48]. The susceptibility of Al-Pd-Mn quasicrystals decreased in the range of 2–200 K with an increase in temperature, whereas in the range of 200–600 K, the susceptibility increased with an increase in temperature [49]. The magnetic susceptibility of a monoquasicrystalline Al_{70.2}Pd_{21.3}Mn_{8.5} sample was measured over the temperature range from 4–1100 K [50].

(iv) Hydrogen storage

The Ti-Zr-Ni icosahedral phase may contain suitable sites for interstitial hydrogen [51-52]. The maximum hydrogen concentration of Ti-Zr-Ni phase powders is approximately 60 at.%, which can be attained by either gaseous-phase or electrochemical loading of hydrogen. The Ti-Zr-Ni icosahedral phase is considered to be a new, promising hydrogen storage material. The substitution of chemical elements in the Ti-based icosahedral phase powders may control hydrogen desorption properties. Both Ti-Hf-Ni and Ti-Zr-Ni alloys were reported to absorb hydrogen without the formation of a detectable crystal hydride phase [53]. The hydrogen storage in nano quasicrystal imbedded in Zr-based amorphes has been reported recently [54].

(v) Mechanical properties of composites

The cylindrical bulk sample of a Zr₆₅Al_{7.5}Cu_{7.5}Ni₁₀Pd₁₀ alloy, the structure of which consists of an almost single icosahedral phase with nanoscale grain sizes of 20–40 nm, shows a better combination of mechanical properties compared with an as-cast glassy sample. The Young's modulus, ultimate tensile strength, 0.2% proof stress, and total percentage elongation (including elastic elongation) are 85 GPa, 1750 MPa, 1640

MPa, and 2.2%, respectively, for the glassy alloy and 88 GPa, 1780 MPa, 1830 MPa, and 3.1%, respectively, for the icosahedral phase-based alloy [55]. However, stoichiometric icosahedral phase-based alloys have high hardness and are extremely brittle, and the icosahedral single phase is unlikely to show plastic deformability. The good mechanical properties of the present alloy are attributed to the residual existence of an intergranular glassy phase, although the volume fraction of the glassy phase is estimated to be less than 5%. The deformation of the icosahedral-based alloy takes place in the intergranular glassy phase along the maximum shear plane. The existence of icosahedral particles can act as a resistant medium against the shear deformation. The good ductility of the glassy layer is also attributed to the localization effect of deformation. The localization generates a multiaxis stress condition, as does an increase in temperature.

Potential applications of quasicrystals

Successful applications of quasicrystals have been very limited. For example, because they are corrosion resistant and have low coefficients of friction, quasicrystals can be applied as a surface coating for frying pans [56]. Another application could be in wear-resistant coatings [57]. Al-Mn-Ce alloys containing nanoicosahedral particles as strong and light materials could be used in surgical blades. Ti-Zr-Ni quasicrystals could be incorporated into hydrogen storage materials. The quasicrystals have been used as a catalytic for hydrogen production and storage recently [58-59].

Quasicrystalline phase in Al-Cu-Fe-Cr

Around 1990, several research groups have found a series of quasicrystals in the family of Al-Cu-Tm alloys (TM=transition metal such as Cr, Mn, Fe, Ru, Or, Co, Rh, or Ni) with composition in the vicinity of Al₆₅Cu₂₀TM₁₅ whether icosahedral or decagonal quasicrystals occur is strongly related to the type of the transition metal. The elements Co, Rh and Ni favour the formation of decagonal quasicrystals, whereas the elements Cr, Mn, Fe, Ru and Or the formation of the icosahedral ones [60-61]. Among the icosahedral quasicrystals, Al₆₅Cu₂₀Cr₁₅ alloy and especially the Al₆₅Cu₂₀Fe₁₅ alloy have been the subject of considerable theoretical and

experimental work which revealed many interesting differences in structure characteristics and thermal stability of two types of icosahedral quasicrystals.

The icosahedral quasicrystal in melt-spun Al-Cu-Cr show electron diffraction spots in the three fold and fivefold directions with a scale factor of $\sqrt{3}$, whereas the Al-Cu-Fe quasicrystals exhibit additional super lattice spots along 5 fold axis at multiples $\sqrt{5}$ and $\sqrt{5}^{-1}$ of the position of the fundamental spots [62]. The former is known to have a P-type quasicrystal and latter F-type one, which can be described projection in three dimensions of the 6D primitive (P) and face-centered (F) cubic lattice respectively [63]. In Al-Cu-Fe quasicrystal the chemical ordering forwards the F-type is so strong that it cannot be suppressed even by rapid quenching. As a result, small domains divided by antiphase boundaries appear in the icosahedral grains of the Al-Cu-Fe alloys. In contrast, the P-type icosahedral quasicrystals in the melt-spun Al-Cu-Cr were observed to be disordered [64]. Besides the structural differences the $\text{Al}_{65}\text{Cu}_{20}\text{Fe}_{15}$ and $\text{Al}_{65}\text{Cu}_{20}\text{Cr}_{15}$ quasicrystals exhibit just opposite thermal stability. It has been established that the Al-Cu-Fe quasicrystals are thermodynamically stable in the high temperature range up to the melting point but become unstable at lower temperatures and transform into their rhombohedral approximants. Contrary to this behavior, the $\text{Al}_{65}\text{Cu}_{20}\text{Cr}_{15}$ quasicrystals were observed to be stable at low temperatures but to decompose at high temperatures. Isothermal annealing above 500°C leads to a eutectoid decomposition of the icosahedral quasicrystals into a hexagonal phase ($a=1.768\text{nm}$ and $c=1.242\text{nm}$) and a long-range vacancy ordered cubic $\sqrt{3}$ -phase ($a=0.877\text{nm}$). At temperature below 450°C , however, the eutectoid decomposition does not occur. The Al-Cu-Cr icosahedral quasicrystals remain unchanged at 450°C even after vary long annealing.

Due to the above-mentioned differences in structure type and thermal stability between Al-Cu-Fe and Al-Cu-Cr quasicrystals, one can expect that successive substitution of Fe by Cr in the Al-Cu-Fe quasicrystals may change their structure from F-type to P-type and weaker their thermal stability as well, whereas the addition of Fe to the Al-Cu-Cr quasicrystals may lead to chemical ordering. Besides, some other phases than the icosahedral phase may also occur. We have synthesized a

nanophase microstructure by mechanical milling (MM) of the quasicrystalline phase in the Al-Cu-Fe-Cr system and to study the phase stability.

Preparation of $\text{Al}_{65}\text{Cu}_{20}\text{Fe}_8\text{Cr}_7$ Alloy

Pure elemental components Al, Cu, Fe and Cr in the atomic composition of $\text{Al}_{65}\text{Cu}_{20}\text{Fe}_8\text{Cr}_7$ were taken for 10gm weight. Then the correctly calculated values for the four elements were weighed precisely using balance with list count 0.0001 gm. These elements were then pressed into a cylindrical pellet by hydraulic pressure (1T/inch) machine. Now the question arises why the compound has been taken in pellet form. The pellet form is taken because each element has different melting points therefore each will melt at different temperature, thereby some of the elements will melt first at their melting point and they will form respective compound which is not the actual objective of our experiment. So in order to avoid this mixture, element is taken in pellet form. The pellet was placed into silica tube and melted to achieve homogeneity using induction furnace (18KW) under argon atmosphere. Then, the as-cast sample was crushed and takes x-ray diffraction (XRD) of the as-cast alloy. After that the sample was kept in a sealing tube made of silica and the tube was taken evacuated and sealed. This sealed tube was then kept at constant temperature for a required time interval. In our case, this temperature around 760°C and the time is 40 hour and annealed alloy further characterized by XRD of the material. After that the material again crushed and then charged in the attrition ball mill with a ball-to-powder ratio of 50 to 1. The attritor has a cylindrical stainless steel balls of 13mm diameter were used. The speed of the mill was maintained at 400 rev min^{-1} . The milling operation was conducted from 1 to 40 h in Toluene medium. Powder obtained after milling for 10h and 40h were investigated by XRD and transmission electron microscopy (TEM) using Technai at 200kv.

Sample preparation for transmission electron microscopic (TEM)

Due to the strong interaction between electrons and matter, the specimens have to be rather thin ($\ll 100\text{nm}$) for TEM investigation. Thus bulk materials have to be thinned to make them electron

transparent. This is done either by simply crushing them or by mechanical grinding and iron milling. Nanoparticles of course are their enough for direct observation. Sample thus prepared were studied by TEM using a Techni G²⁰ at 200kV electron microscope employing imaging and diffraction modes. For TEM studies of the as cast as well as ball milled powder particles, such particles which floated on the surface of distilled water and hence were expected to be thin were picked up. These were mounted on copper grid of 300 mesh sizes pre-coated with formvar.

Structural Characterization through X-ray diffraction

The as cast and mechanically milled sample were subjected to structural characterization employing powder XRD Philips PW 1710 diffractometer with CuK_α radiation $\lambda = 1.5418\text{\AA}$. The experimental conditions such as rating of x-ray generator (30 KV, 20 mA) and other diffractometer parameters such as scanning speed were kept constant for all diffraction experiments performed on different samples.

The grain size and the lattice strain of the sample can be calculated from the integral width of the physical broadening profile. Cauchy and Gaussian components can be obtained from the ratio of full width at half maximum intensity (2ω) and integral breadth (β). In a single line analysis the apparent crystallite size ' D ' and strain ' e ' can be related to Cauchy (β_c) and Gaussian (β_G) widths of the diffraction peak at the Bragg angle θ ;

$$D = k\lambda / \beta_c \cos \theta \quad (\text{i})$$

$$\text{and } e = \beta_G / 4 \tan \theta \quad (\text{ii})$$

The constituent Cauchy and Gaussian components can be given as

$$\beta_c = (a_0 + a_1\psi + a_2\psi^2) \beta$$

$$\beta_G = (b_0 + b_{1/2}(\psi - 2/\pi)^{1/2} + b_1\psi + b_2\psi^2) \beta$$

where a_0 , a_1 and a_2 are Cauchy constants, b_0 , $b_{1/2}$, b_1 and b_2 are Gaussian constants and $\psi = 2\omega/\beta$ where β is the integral breadth obtained from XRD peak. The values of Cauchy and Gaussian constant have been taken from the table of Th. H. de Keijser et al. [65]. $a_0 = 2.0207$, $a_1 = 0.4803$, $a_2 = 1.7756$; $b_0 = 0.6420$,

$b_{1/2} = 1.4187$, $b_1 = 2.2043$, $b_2 = 1.8706$) from these, we have calculated the crystallite size D and the lattice strain ' e ' for the milled Al₆₅Cu₂₀Fe₈Cr₇ alloy.

Figure 1 shows the XRD pattern obtained from the as cast Al₇₀Cu₂₀Cr₈Fe₇ alloy. The diffraction patterns have been indexed on the basis of decagonal phase as well as orthorhombic crystalline phase with $a = 23.65 \text{\AA}$, $b = 12.28 \text{\AA}$ and $c = 32.45 \text{\AA}$. The decagonal phase can be indexed by using six independent indices as proposed by Mukhopadhyay and Lord [66]. The indexing and calculated standard deviations (SD) in d value have been given in table 1. After annealing treatment of Al₇₀Cu₂₀Cr₈Fe₇ as-cast material at a temperature 760 °C for 40 hrs, it is noted that the centre of the broad peak, split in to two peaks (Fig.2). The intensity and amount of crystalline peak going to be negligible during annealing, suggesting that the transformation from the crystalline phase to quasicrystalline phase take place. The sharpness and the intensity of the peaks were improved significantly. This can be attributed to the ordering, annihilation of defects, strain relaxation, and grain coarsening. The indexing and calculated standard deviation in d values has been given in table 2. Fig.3(c) shows the XRD pattern from 40 h MM powder exhibiting broadening of the peaks belonging to the B2 phase. For the comparison the XRD of as cast and annealed alloys have been also given in Fig. 3(a-b). The effect of the reduced size of the crystallites and lattice strain can be observed on the overall peak intensity and broadening, which is obvious after 40h of milling. The B2 phase is a CsCl structure in intermetallics, its unit cell contains two different atoms located respectively on the vertex and the centre of a cube. Its lattice parameter is 0.31 nm. It can be seen that, the peak intensity of the milled sample are decreased and the peak are significantly broadened, suggesting that a large amount of defects were introduced into the samples by mechanical attritor and finally the reduction of crystallite size. Sufficient information about the changes in grain size and lattice strain can be gained from the integrated width of the peak. We can get the physical profile of the 40h milled powder, which is the convolution of size broadening with the strain broadening profile, by removing the

instrumental broadening effect from the measured intensity profile. The instrumental broadening profiles, determined by means of the Si reference sample in the present work, are revealed to be Gaussian function. Both theory and experiment support the approximation of size broadening profiles by a Lorentzian function and strain broadening by a Gaussian function. The crystallite size of the sample was being calculated from the integral width of the physical broadening profile. The crystallite size after 40 h of milling time is 18 nm. It is known that the high-energy ball milling technique introduces defects, disordering and reduction of grain size, and thereby destabilizes the ordered phase. However in the present case, it is interesting to note that the vacancy ordered phase has not been formed even after MM of 40 h.

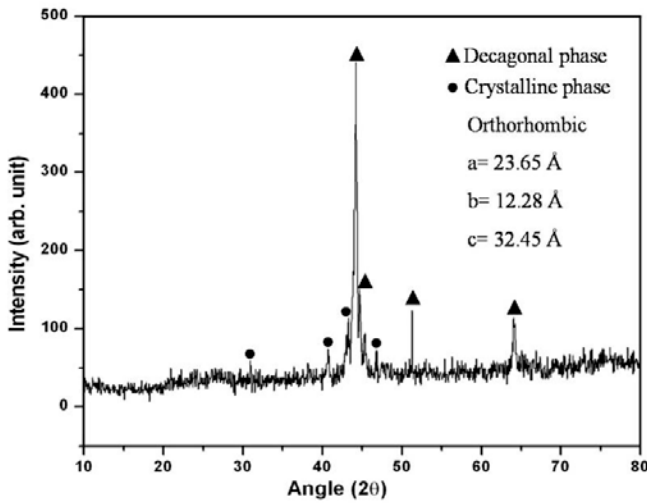


Figure 1

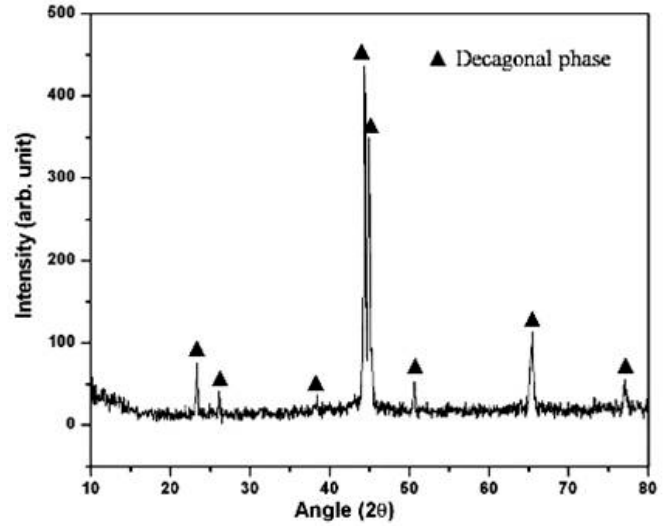


Figure 2

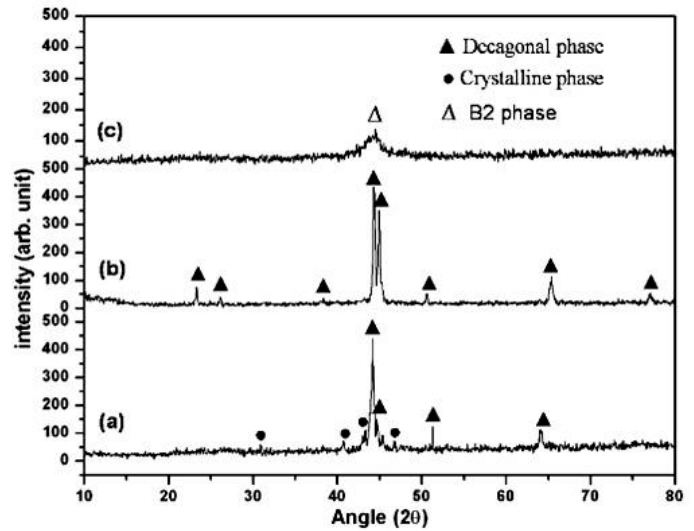


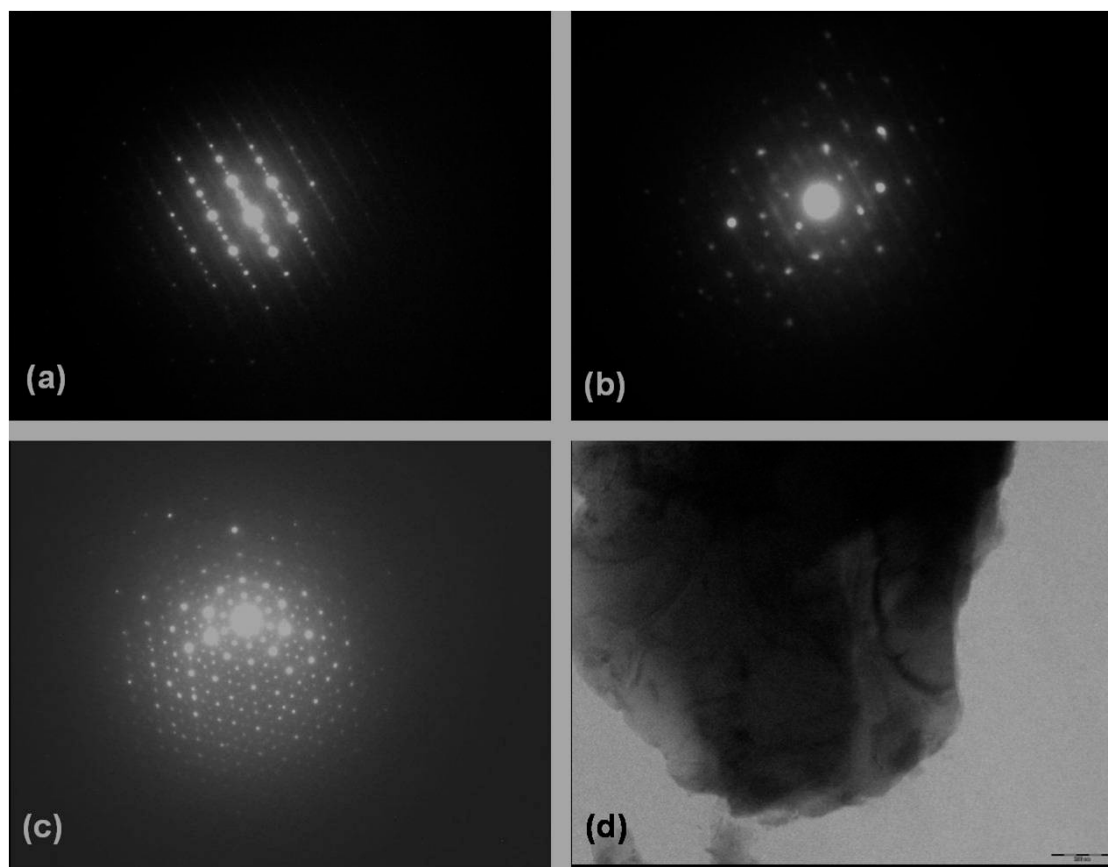
Figure 3

Table 1. Comparison of standard d values and observed d values by XRD of as-cast alloy

Observed d values (Å ⁰)	For decagonal phase (Å)	For crystalline phase (Å)	Δd for decagonal phase (Å)	Δd for crystalline phase (Å)	Indexing
2.2143 (●)		2.2182		0.0039	828
2.0895 (●)		2.0566		0.329	838
2.0472 (▲)	2.042		0.0052		102202
1.9971 (▲)	1.995		0.0021		000004
1.7797 (▲)	1.797		0.0173		111104
1.4520 (▲)	1.450		0.002		211104

Table 2. Comparison of standard d values and observed d values by XRD of annealed sample

Observed d values (Å)	For decagonal phase (Å)	Δd for decagonal phase (Å)	Indexing
3.8256	3.8000	0.0256	101100
3.4204	3.4160	0.0044	111100
2.3513	2.3460	0.0005	102200
2.0463	2.0420	0.0013	102202
2.0217	2.0330	0.0113	000004
1.8081	1.7970	0.0066	111104
1.4288	1.4253	0.0035	211104
1.2397	1.2340	0.0027	303220

**Figure 4**

Morphology and Electron diffraction analysis/ Characterization

The rigorous transmission electron microscopic investigation obtaining by selected area diffraction

patterns and microstructural features at different stages have been carried out. Fig.4 (a)-(c) show typical selected area diffraction(SAD) patterns obtained with the electron beam carefully oriented parallel to the twofold (a-b) and fivefold (c)

symmetry axes. Twofold symmetry selected area electron diffraction patterns of decagonal particles take at two different positions. (Fig.4 (a-b)). However, some of the wider spots were found to be slightly elongated, especially in the twofold symmetry diffraction patterns. The two fold diffraction pattern of decagonal phase shows the presence of streaking along the aperiodic direction as shown in Fig. 4(a-b). This streaks can be interpreted due to disordering along decagonal axis. Typical SAD along five-fold axis is shown in fig.4(c). Fig. 4 (d) brings out a representative microstructure of typical decagonal particles. The microstructure is a single-phase decagonal quasicrystal having two different rotational axes. Fig.5 (a) and (b) are bright-field and dark-field TEM images obtained from the powder sample milled for 40 h. Some of the powder particles were electron transparent near the edges. The very fine grain size of the B2 phase, of the order of 10-20 nm, is evident. Figure 5 (c) shows a typical ring diffraction pattern obtained from the sample. These rings can be indexed as the disordered B2 that is a bcc phase with a lattice parameter of 0.3 nm. This is consistent with the observations from the XRD patterns.

Essentially, the role of ball milling is to lead to the enhancement of thermally activated diffusion by generating a large number of defects as well as forcing the atoms or groups of atoms to move from place to place. As it is possible to obtain a nanoscale microstructure, the rate of diffusion during subsequent thermal heat treatment is quite high, which may lead to the formation of equilibrium or stable phases in the system. In the present investigation it was found that the QC phase was unstable during milling, transforming to nanocrystalline of the B2 phase.

Conclusions

In this paper, we focused on synthesis of quasicrystal by different processes. The stability was discussed in terms of Hume-Rothery rules for the metastable and stable quasicrystal in terms of phason disorder. The different properties were also discussed. We have also discussed a particular example of $\text{Al}_{65}\text{Cu}_{20}\text{Fe}_8\text{Cr}_7$ decagonal quasicrystalline alloy. In this case, the as cast material shown dominantly decagonal phase along with orthorhombic minority phase. The alloy

becomes single decagonal phase after annealing in vacuum at 760°C for 40 hours. The decagonal $\text{Al}_{65}\text{Cu}_{20}\text{Fe}_8\text{Cr}_7$ alloy is unstable under high energy ball milling, transforming to a nanocrystalline B2 phase. The repeated impact between the balls and powders appears to cause the generation of various types of defects including phason type. Consequently due to the defects generated during milling, the structural transformation to a crystalline phase takes place. On milling up to 40 h, the grain refinement is achieved and the grain size reached to a minimum of 18 nm.

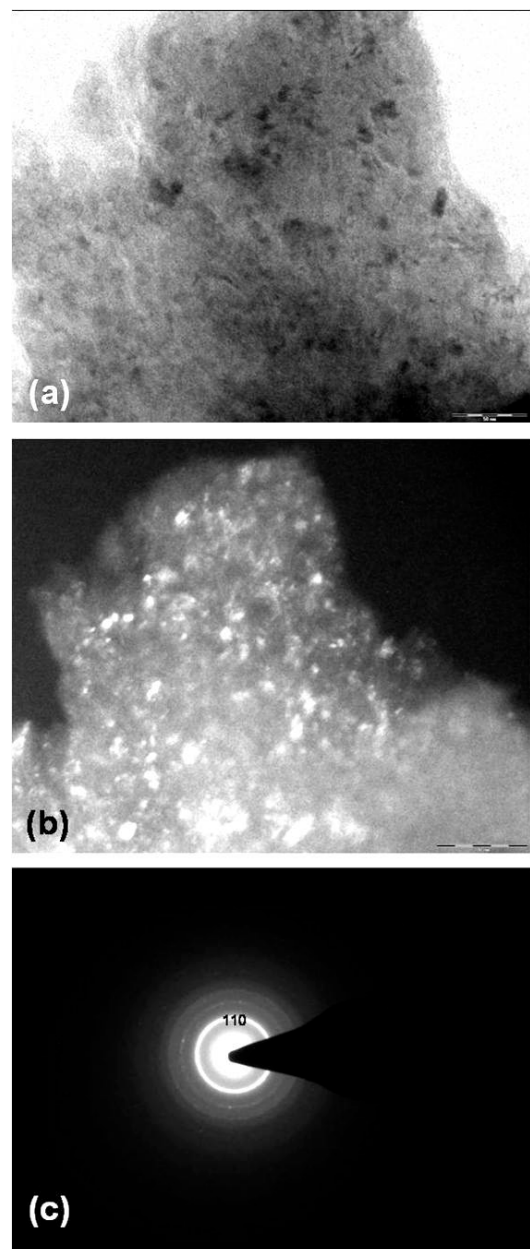


Figure 5

Acknowledgements

The authors gratefully acknowledge the discussion with all their collaborators, who have immensely contributed to the collaborative research work, a part of which has been discussed in this review. Authors would like to thank Dr. H. R. Sharma, Prof. R. McGrath, and Prof. R. Tamura, Prof. A.P.Tsai, Prof. R. S. Tiwari, Prof. R. K. Mandal, Prof. B. S. Murty, Dr M.A. Shaz, and Dr. Kalpana Awasthi for many collaborative work and stimulating discussions. Authors sincerely acknowledge the invitation and encouragement from Prof. G. V. S. Sastry for giving them the opportunity of completing this review.

References

- [1] D. Shechtman, I. Bleeh, D. Gratias and J.W. Cahn, A Metallic Phase with Long- Ranged Orientational Order and Broken Translational Symmetry, *Phys Rev Lett* 53, 1951, 1984.
- [2] L. Bendersky, *J. De Physique* 47, C3-457, 1986.
- [3] J. A. Sekhar and T. Rajasekharan, *Nature* 320, 153, 1986.
- [4] W. A. Cassada¹, G. J. Shiflet¹ and S. J. Poon, Quasicrystalline grain boundary precipitates in aluminium alloys through solid-solid transformations, *Journal of Microscopy*, 146, 323, 1987.
- [5] K.G. Kreider, Process for producing icosahedral materials, US Patent 4,772,370, 1988.
- [6] J. A. Knapp and D. M. Follstaedt, Formation of Icosahedral Al(Mn) by Directed Energy Processes, *Phys. Rev. Lett.* 55, 1591, 1985.
- [7] D. M. Follstaedt and J. A. Knapp, Formation of Icosahedral Al(Mn) by Pulsed Surface Melting, *MRS Proceedings*, MRS Proceedings, 58, 1985.
- [8] W. A. Cassada, G. J. Shiflet, and S. J. Poon, Formation of an Icosahedral Phase by Solid-State Reaction, *Phys. Rev. Lett.* 56, 2276, 1986.
- [9] M. D. Ball and D. J. Lloyd, *Scr. Met.* 19, 1065, 1985.
- [10] W.A. Cassada, G.J. Shiflet, E.A. Starke Jr, The effect of germanium on the precipitation and deformation behavior of Al₂Li alloys, *Acta Metallurgica*, 34, 367, 1986.
- [11] J. Eckert, L. Schultz and K. Urban, Phase Transitions and Quasi-Crystal Formation in Al-Cu-Mn Induced by Ball Milling, *Europhysics Letters*, 13, 349, 1989.
- [12] J. Eckert, L. Schultz and K. Urban, *Acta Metall. Mater.* 39, 1497, 1991.
- [13] P. Barua, V. Srinivas and B.S. Burty, *Phil. Mag. A*, 80, 1207, 1985.
- [14] N. K. Mukhopadhyay, J. Bhatt, A.K. Pramanik et al., *J. Mater. Sci.* 39, 5155, 2004.
- [15] Y. Saito, Ho S. Chen and K. Mihama, Icosahedral quasicrystal produced by gas evaporation of an Al-Mn alloy, *Appl. Phys. Lett.* 48, 581, 1986.
- [16] A. P. Tsai, A. Inoue, Y. Bizen and T. Masumoto, *Acta Metall.* 37, 1443, 1989.
- [17] S. Ebalard and F. Spaepen, *Journal of Materials Research*, 5, 62, 1990.
- [18] H. Zhang and K. Urban, *Phil. Mag. Lett.* 66, 209, 1990.
- [19] S. S. Kang and J. M. Dubois, *Europhys. Lett.* 18, 45, 1992.
- [20] N.K. Mukhopadhyay, G. V. S. Sastry and G.C. Weatherly, *Phil. Mag. A*, 80, 1795, 2000.
- [21] T.P. Yadav, N.K. Mukhopadhyay, R.S. Tiwari and O. N. Srivastava, *J. for Sust. Devel.* 15, 259, 2007.
- [22] T.P. Yadav, N.K. Mukhopadhyay, R.S. Tiwari and O. N. Srivastava, *Trans I. Inst. Metall.* 58, 1169, 2005.
- [23] N. Yu, R. Portier, D. Gratias, K. Yu-Zhang and J. Bigot, Al₆CuLi₃-T₂: A Stable icosahedral Phase, *Materials Science Forum*, 22- 24, 579, 1987.
- [23] A.P. Tsai, A. Inoue and T. Masumoto, *Jap. J. appl. Phys.*, 26, L1505, 1987.
- [24] A.P. Tsai, A. Inoue and T. Masumoto, *Jap. J. appl. Phys.* 27, L1587, 1987.
- [25] A.P. Tsai, A. Inoue and T. Masumoto, *Mater Trans. JIM* 30, 150, 1989.
- [26] A.P. Tsai, J.Q. Guo, E. Abe, H. Takakura and T. J. Sato, *Nature* 408, 537, 2000.
- [27] A.P. Tsai, A. Inoue and T. Masumoto, *Mater Trans. JIM* 30, 300, 1989.
- [28] A. P. Tsai, A. Inoue and Y. Yokoyama and T. Masumoto, *Mater. Trans. JIM.* 31, 98, 1990.
- [29] A. P. Tsai, *J. Non-Cryst. Solids*, 334-335, 317,

2004.

- [30] L. Pauling, *Phys. Rev.* 54, 899, 1938.
- [31] K. Edagawa, *Dislocations in quasicrystals*, *Materials Science and Engineering: A*, 309–10, 528, 2001.
- [32] A. P. Tsai, A. Inoue, Y. Yokoyama and T. Masumoto, *Japan J. Appl. Phys.* 29, L1161, 1990
- [33] Y. Yokoyama, Y. Yamada, K. Fukaura, H. Sunada and A. Inoue, *Jpn. J. Appl. Phys.*, 36, 6470, 1997.
- [34] D. Levine and P. Steinhardt, *J. Phys. Rev. B* 34, 596, 1986.
- [35] A. Yamamoto, K. Kato, T. Shibuya and S. Takeuchi, *Phys. Rev. Letters* 65, 1603, 1990.
- [36] K. Urban, M. Feuerbacher and M. Wollgarten, *Mater. Res. Soc. Bulletin*. 22, 65, 1997.
- [37] K. Urban, M. Feuerbacher, M. Wollgarten, M. Bartsch, U. Messerschmidt, *Mechanical Properties of Quasicrystals*, Springer Series in Solid-State Sciences, 126, 361, 1999.
- [38] S. Takeuchi and K. Kimura, *J. Phys. Soc. Jpn.* 56, 982, 1987.
- [39] G. D. Schaaf, J. Roth and H. R. Trebin, *Dislocation motion in icosahedral quasicrystals at elevated temperatures: Numerical simulation*, *Philosophical Magazine*, 83, 2449, 2003.
- [40] M. A. Chernikov, A. Bianchi and H. R. Ott., *Phys. Rev. B* 51, 153, 1995.
- [41] M. Tanaka, K. Tsuda, M. Terauchi, A. Fujiwara, A. P. Tsai, A. Inoue and T. Masumoto, *J. Non-Cryst. Solids* 153, 98, 1993.
- [42] R. Tamura, K. Edagawa, Y. Murao, S. Takeuchi and K. Suzuki, *Phys. Rev. B*, 68, 74105, 2001.
- [43] S. J. Poon, *Electronic properties of quasicrystals an experimental review*, *Advances in Physics*, 41, 303, 1992.
- [44] J. Dolinsek, S. Vrtnik, M. Klanjek, Z. Jaglicic, A. Smontara, I. Smiljanic, A. Bilusic, Y. Yokoyama, A. Inoue and C. V. Landauro, *Physical Review B*, 76, 054201, 2007.
- [45] S. Kashimotoa, S. Matsuob, H. Nakanob, T. Shimizuc, T. Ishimasad, *Magnetic and electrical properties of a stable Zn-Mg-Ho icosahedral quasicrystal*, *Solid State Communications*, 109, 63, 1998.
- [46] T. J. Sato, J. Guo and A. P. Tsai, *Magnetic properties of the icosahedral Cd-Mg-rare-earth quasicrystals*, *J. Phys.: Condens. Matter*, 13, 2000, L105.
- [47] I.R. Fisher, M.J. Kramer, T.A. Wiener, Z. Islam, A.R. Ross, T.A. Lograsso, A. Kracher, A.I. Goldman, P.C. Canfield, *Philos. Mag. B*, 79, 1673, 1999.
- [48] I.R. Fisher, M.J. Kramer, Z. Islam, T.A. Wiener, A. Kracher, A.R. Ross, T.A. Lograsso, A.I. Goldman and P.C. Canfield, *Mater. Sci. Eng. A* 294–296, 10, 2000.
- [49] J.Q. Guo, T.J. Sato, E. Abe, H. Takakura and A.P. Tsai, *Philosophical Magazine Letters*, 80, 495, 2000.
- [50] V. Simonet, F. Hippert, M. Audier, and G. Trambly de Laissardière, *Origin of magnetism in crystalline and quasicrystalline AlMn and AlPdMn phases*, *Phys. Rev. B* 58, R8865, 1998.
- [51] A. Taksaki and K.F. Kelton, *International Journal of Hydrogen Energy*, 31, 183, 2006.
- [52] Rohit R. Shahi, T.P. Yadav, M.A. Shaz, O.N. Srivastava, S. van Smaalen, *Effect of processing parameter on hydrogen storage characteristics of as quenched Ti₄₅Zr₃₈Ni₁₇ quasicrystalline alloys*, *International Journal of Hydrogen Energy*, 36, 592, 2011.
- [53] P.C. Gibbons, R.G. Hennig, V.T. Huett, K.F. Kelton, *Ti-Zr-Ni and Ti-Hf-Ni quasicrystals and approximants as hydrogen storage alloys*, *J. Non-Cryst. Solids* 334–335, 461, 2004.
- [54] D. Singh, R. R. Shahi, T.P. Yadav, R.K. Mandal, R.S. Tiwari, O.N. Srivastava, *Hydrogenation of (Zr_{69.5}Al_{7.5}Cu₁₂Ni₁₁)_{100-x}Ti_x quasicrystalline alloys and its effect on their structural and microhardness behavior*, *Journal of Non-Crystalline Solids* 380, 11, 2012.
- [55] A. Inoue and H. Kimura, *Mater. Sci. Engng A*, 286, 1, 2000.
- [56] N. Rivier, *Non-stick quasicrystalline coatings*, *Journal of Non-Crystalline Solids*, 153–154, 458, 1993.
- [57] Jean-Marie Dubois, *So Useful, Those Quasicrystals*, *Israel Journal of Chemistry*, 51, 1168, 2011.

- [57] Sunita K. Pandey, T.P.Yadav and O.N. Srivastava, Catalytic application of Al-Cu-Fe quasicrystal for Hydrogen storage, to be communicated, 2014.
- [59] T.P.Yadav, Sunita K. Pandey and O.N. Srivastava, Leaching of mechanically activated Al-Cu-Fe icosahedral quasicrystalline phase and its catalytic application, *Acta Physica Polonica A* (2014) In press
- [60] Jean-Marie Dubois, *Useful Quasicrystals*, publisher; World Scientific 2005. ISBN: 978-981-02-3254-2.
- [61] T.P.Yadav and O.N. Srivastava, *Book; Formation and phase stability of some Albased quasicrystals and related nano phases*, (2012) publisher Lap Lambert Academy Publishing, Heinrich,
- [62] W Liu, U Köster, F Müller and M Rosenberg, *Phys. Status Solidi (a)*132, 17, (1992).
- [63] G. Bonhomme M. LeMieux P. Weisbecker V.V. Tsukruk and J.M. Dubois, *Journal of Non-Crystalline Solids*, 334&335, 532 (2004).
- [64] G. Rosas and R. Perez, *Journal of Materials Science* 32, 2403, 1997.
- [65] Th. H. de Keijser, J. I. Langford, E. J. Mittemeijer and A. B. P. Vogels, *J. Appl. Cryst.* 15, 308, 1982.
- [66] N. K. Mukhopadhyay and E. A Loard, *Acta. Cryst. A.* 58, 424, 2002.

Interface Structure of Inversion Domain Boundary: A Case Study on Polycrystalline GaN

Joysurya Basu and R. Divakar

Physical Metallurgy Group, Indira Gandhi Centre for Atomic Research, Kalpakkam-603102, TN, India, E-mail: jbasu@igcar.gov.in

Abstract

It has been demonstrated that interfaces other than $10\bar{1}0$ plane may exist in inversion domains in GaN. Inversion domain pipes are similar to inversion domains where two interfaces lie very close to one another. A diffraction contrast mechanism under two beam condition from inversion domain pipes has been proposed. Whenever the inversion domain pipes lie over a fault plane contrast reversal in the fault fringes also takes place leading to an alternating bright and dark contrast for the inversion domain pipes. Inversion domains and anti-phase domains are both related with a lattice translation. However, inversion domains occur in ionic crystals with the cation to anion bonds arranged in a particular direction. In case of inversion domains, additional translations become necessary in order to minimize the interface energy.

Key Words: Defects; Interfaces; Hydride vapor phase epitaxy; Nitrides; Sapphire; Semiconducting III-V materials.

Introduction

GaN films have been intensively studied over the last decade because of its large direct band gap (3.2-6.3 eV) and potential applications in opto-electronic devices [1-2]. However, it has not been possible till date to synthesize bulk or defect-free thick film of GaN because of the unavailability of a suitable substrate [3]. The tolerance of defect density in GaN is considerably high compared to the other semiconductors so far their functional properties are concerned [4]. However, defect density significantly reduces the life time and it is the major bottle neck to synthesize bulk single-crystal GaN. It is not quite understood as to how the defects affect the functional properties of this semiconductor in the pure and doped form.

Of several substrates, that have been tried for growth of GaN films, c-plane sapphire is the most suitable one [5] where hexagonal GaN grows with a particular epitaxial relationship such that $[0001]_{\text{GaN}} \parallel [0001]_{\text{Sapphire}}$ and $[11\bar{2}0]_{\text{GaN}} \parallel [10\bar{1}0]_{\text{Sapphire}}$ and there is a lattice mismatch of ~16%. In order to reduce the defect density caused by the lattice mismatch and to reduce the interfacial strain, a number of techniques

have been devised to prepare the substrate surface [6].

Among the several possible structural defects, dislocations have been studied most intensively. Dislocations are generated at the film substrate interface which may propagate across the film from interface to the surface. The dislocations can be pure screw type with $b = [0001]$, pure edge type with $b = [11\bar{2}0]$ and/or mixed type with $b = [11\bar{2}3]$. Among the planar defects, stacking faults and twins have been studied intensively. The planar defects, which have received relatively less attention are inversion domain boundaries and stacking mismatch boundaries [4].

Inversion domain boundaries (IDB) are those in which the polarity of the wurtzite GaN crystal is inverted in the other side of the boundary. Wurtzite GaN has hexagonal structure where half the tetrahedral voids are filled with nitrogen ions. In this structure positively charged Ga ions layers and negatively charged nitrogen ion layers are alternately arranged along $[0001]$ direction. This introduces polar nature in the crystal i.e. Ga-N bonds are either pointing upward or downward. As $[0001]$ direction of GaN is always perpendicular to the

(0001) surface of sapphire, the wurtzite crystal may end up either with Ga-polar surface or with N-polar surface. Polarity inversion i.e. change in direction of the Ga-N bonds may occur locally leading to the formation of the inversion domains. Polarity inversion is supposed to affect the optical and electronic properties of the GaN films and suitable microstructural tailoring of these boundaries may be exploited for designing lateral polarity heterostructures. Stacking mismatch boundaries occur when stacking sequence in the GaN crystal changes between two parts of the crystal. On a hexagonal close-packed array of Ga ions, next layer can be placed in two ways i. e. if the first layer is considered as 'A' then the second layer of Ga ions can take the 'B' sites or the 'C' sites. Stacking mismatch boundaries form when one part of the crystal is stacked as ABAB.... And the other part of the crystal is stacked as ACAC.....In both the cases of inversion domain boundaries or stacking mismatch boundaries local distortion in ionic coordination takes place which might lead to the formation of defects [7].

Since the inception of GaN as a potential optoelectronic material, considerable research efforts have gone towards the search of suitable substrate, manipulating the substrate surface, growth of thicker GaN films, study of defects mainly oriented towards the study of dislocations. In this respect inversion domains have received relatively less attention. Almost always, it has been assumed that the inversion domains are bounded by $10\bar{1}0$ surfaces. The origin of this kind of defects, their atomic structure is not clearly understood and the existing models are not enough to explain all the experimental observations. The aim of this paper is to review all the existing morphological and structural models of inversion domains. A new structural model of interaction of inversion domain boundaries with stacking faults and the mechanism of contrast formation under two-beam diffraction condition have been proposed. Finally a comparison has been drawn between inversion domain boundaries and anti-phase boundaries (APB).

Experimental Technique

Polycrystalline GaN has been grown on c-plane sapphire substrate by hydride vapor phase epitaxy (HVPE) by suitably optimizing the processing

conditions. Growth of GaN by HVPE has been reported before in literature. Plan-view and cross-sectional TEM samples were prepared by conventional techniques. The defects have been characterized by Tecnai T12 transmission electron microscope operated under 120 kV. Diffraction contrast imaging techniques have been used to understand the defect and its interaction with the existing stacking faults.

Results

Mainly two morphologies of inversion domains have been studied in the present work i.e inversion domains and inversion domain pipes. Bright field image of an inversion domain has been shown in fig 1(a & b). The inversion domain has many facets and fringe-contrast can be observed along some of the facets whereas one facet is almost edge on (marked with white arrow in figure 1c). Fringe contrast along certain facets indicates that they are inclined to the incident electron beam. It can be concluded from the image that all the facet planes are not the variant of the same plane. The domain is totally invisible in the dark field image with the $10\bar{1}0$ reflection (Fig. 1b). The invisibility of the domain with this reflection indicates a possible translation vector along $[0001]$ direction. In order to prove the inverted nature of the domain, the same region of the sample was tilted to excite the $10\bar{1}1$ reflection. The corresponding dark field image is given in fig. 1c. In this image fringe-contrast along many of the facets can be seen, one of the facets is almost edge on and a few are close to the edge on position. The visibility of this domain with $10\bar{1}1$ reflection further supports the probability of having a translation vector along $[0001]$ direction. In order to prove the inverted nature of the domain, CBED pattern with $10\bar{1}1$ reflection was recorded inside and outside of the domain (Fig 1c inset). For hexagonal GaN, $10\bar{1}1$ is a non-centrosymmetric reflection and the contrast within the reflection disc from inside and outside the boundary is almost complementary. This observation confirms the inverted nature of the domain with respect to the parent crystal. This near complementary contrast is observed in-spite of having thickness difference inside and outside of the domain and from the edge of the sample, as evident from the thickness fringes.

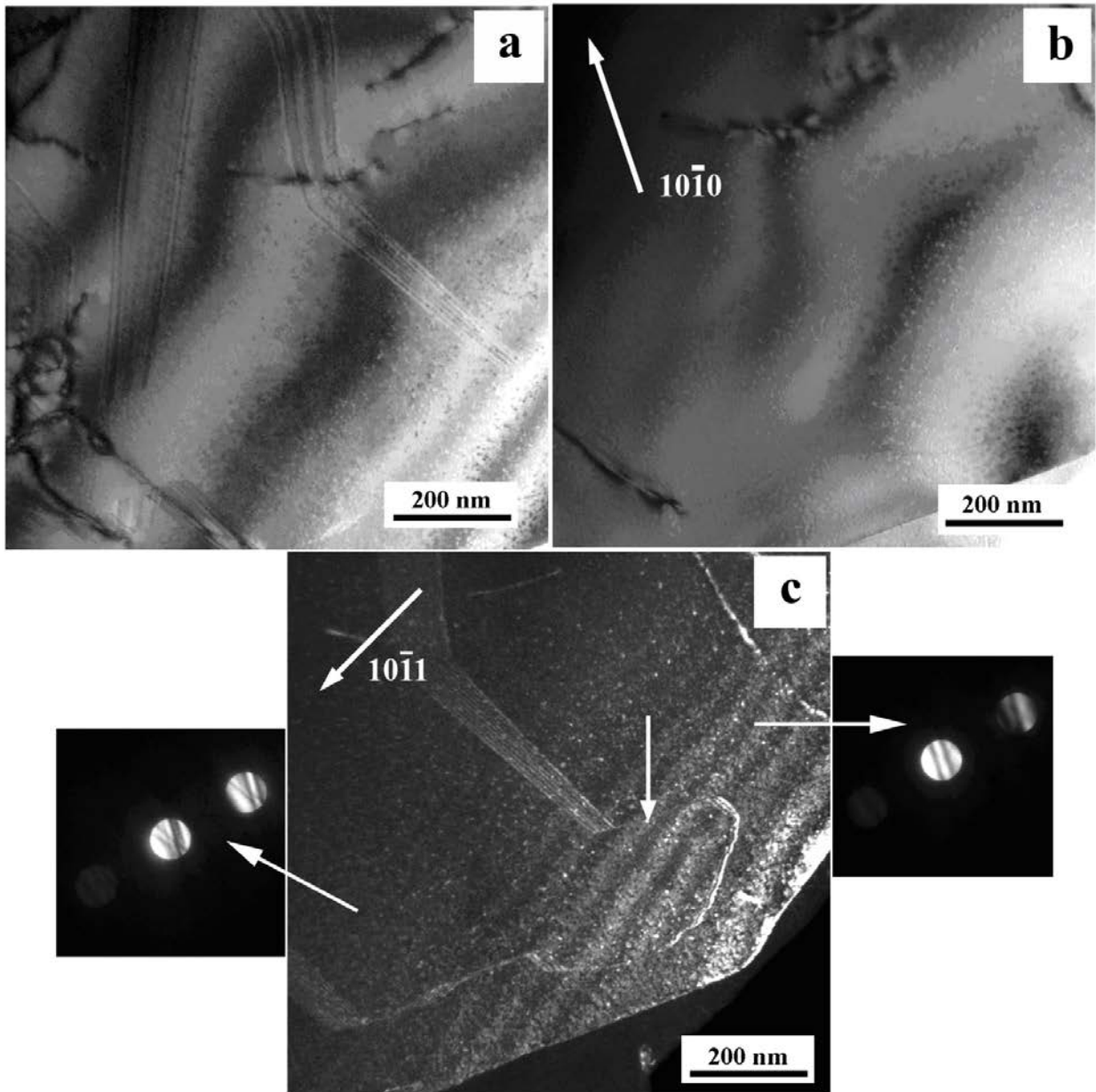


Figure 1. (a) Inversion domain in GaN with multiple facets. Some of the facets show fringe contrast where as some of the facets are edge on. (b) Dark-filed image of the same domain with 10-10 reflection. The domain is invisible under imaging condition, indicating a possible translation along 0001 direction. (c) Dark-field image of the same domain with 10-11 reflection. Some of the facets show fringe contrast, some of them are edge on and some of them are nearly edge on. CBED patterns with 10-11 reflection from inside and outside the domain (marked with arrow) show complementary contrast.

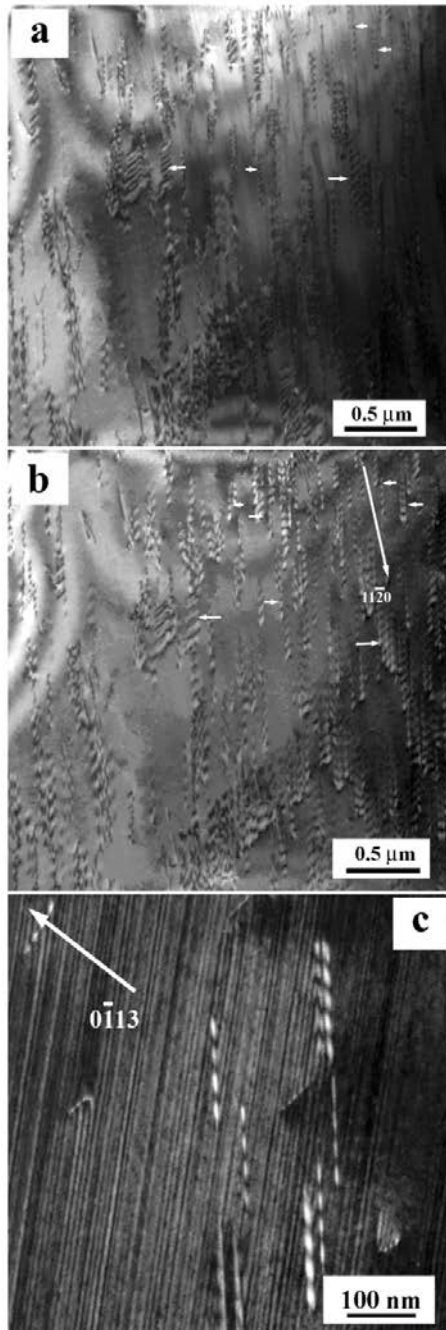


Figure 2. (a) Bright-field (b) dark-field image of the inversion domain pipes in GaN with $11\bar{2}0$ reflection. Complementary contrast in the bright-field and the dark-field image (marked with arrow) can be observed. (c) Dark-field image of the inversion domain pipes with $0\bar{1}13$ reflection. A number of parallel fringes can be seen. The bright and the dark fringes of the inversion domain pipes are also synchronous with the parallel fringes indicating that the pipes lie parallel to the planar fault.

The other inversion domain morphology that has been studied in the present work is in the form of pipes. In GaN inversion domain pipes appear as straight long chains with alternating bright and dark fringes (Fig. 2). The domain pipes are typically very narrow and 200 nm to about $1\mu\text{m}$ long. Complementary contrast along these domain pipes can be observed in bright field and dark field image when imaged with $11\bar{2}0$ reflection. Quite a few locations with complementary contrast have been marked with arrows in fig. 2 (a & b). Dark field image of the domain pipes with $0\bar{1}13$ reflection is shown in fig. 2c. In this image alternating bright and dark fringes along the inversion domain pipes and a series of parallel fringes can be observed. The alternating bright and dark contrast along the domain pipes is synchronous with the parallel fringes in the micrograph. It can be concluded that the inversion domain pipes are inclined and the defect that gives rise to the fringes are also inclined and their angle of inclination with the horizontal plane of the sample is same. This strongly indicates that these inversion domain pipes lie parallel to the fault plane of the sample. The fringes are parallel to the $11\bar{2}0$ direction.

Bright field and dark field image of the same region with $10\bar{1}3$ reflection is shown in fig.3 (a and b). Due to extensive tilting the domain pipes change their appearance and the fringes are still visible. In both the images whenever the straight parallel fringes cross one inversion domain pipe the change in contrast can be observed. Some of the locations are marked with arrows. Complementary contrast can be observed in the bright filed and the dark filed images. Many of the inversion domain pipes make 30 degree angle with the fringes. As the fringes are parallel to the $11\bar{2}0$ direction it can be concluded that the interface plane is $10\bar{1}0$. In some cases the interface is curved. In that case it may not be parallel to the $10\bar{1}0$ plane.

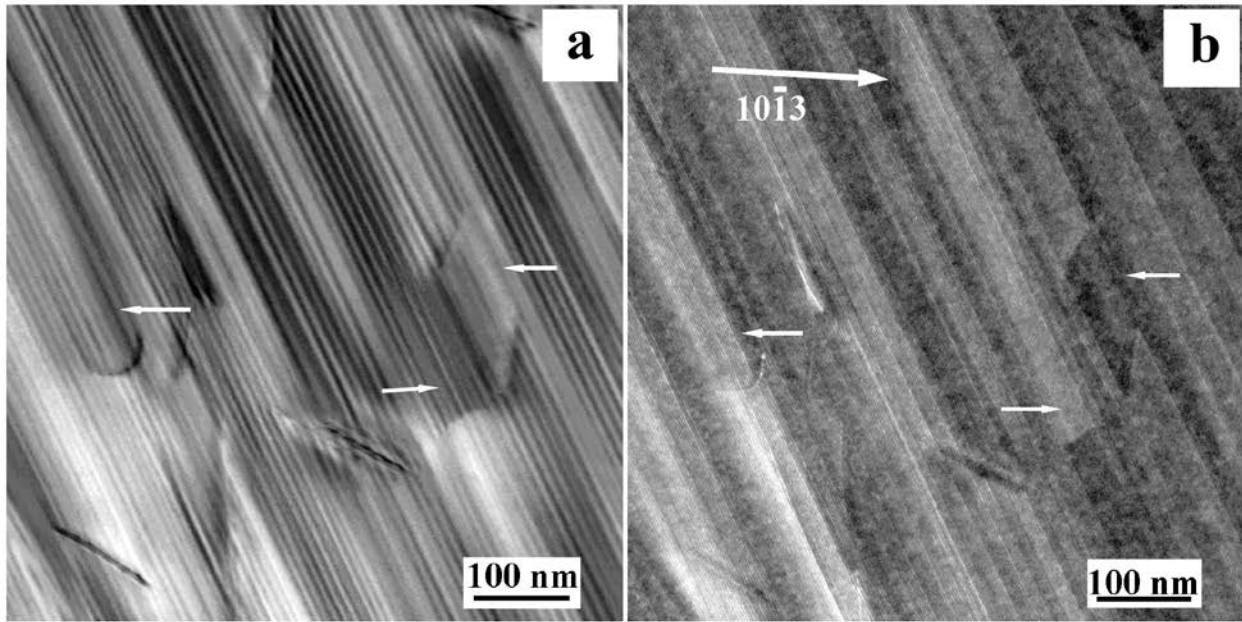


Figure 3. (a) Bright-field (b) dark-field image of the inversion domain pipes with 10-13 reflection. Complementary contrast in the bright- and the dark-field images and the change in contrast across the inversion domain boundary in the same image can be observed.

Discussion

A mechanism of contrast generation from an inversion domain lying on or parallel to the planar fault plane can be proposed. When the planar fault is inclined to the beam direction, it will produce a number of parallel fringes in the image. Whenever the inversion domain pipe lies on or parallel to the fault plane, it will also produce the similar fringes and due to the inverted nature of the domain the contrast of the fringes will be complementary to that of the planar fault. As a result of this the contrast from the inversion domain pipe will change synchronously with the fringes from the planar fault. Depending on the orientation of the inversion domain with respect to the planar fault, the planar fault fringe orientation with the inversion domain will change.

Inversion domain is a widely encountered defect in non-centrosymmetric crystals and the structure of inversion domain boundaries has been studied for decades. The first model, known as Austerman Model, was proposed in 1966 [8]. According to this model, anion sublattice remains continuous and the cations change their position from one type of

tetrahedral site to another across the interface. According to Holt model, cations and anions change their positions in two sublattices across the boundary [9]. Northrup et al. in 1996 [7] and Potin et al. 1997 [10] proposed a variant to the Holt Model, which involves a $c/2$ translation along the c -axis in order to avoid the Ga-Ga and N-N bonds. All these models invariably assume that the inversion domain

boundary exists along the $10\bar{1}0$ surface and in other words they eliminate the possibility of existence of inversion domain boundaries along other planes. In this work it is clearly seen that the inversion domain boundary may exist along planes which are not a variant of $10\bar{1}0$. The detailed atomic structures of inversion domain boundaries along other surfaces remain to be understood.

Based on the model of inversion domain boundary along $10\bar{1}0$ interfaces it has been predicted and experimentally observed that the termination mechanism of inversion domains should be associated with stacking faults. The structural interaction of inversion domains and the stacking fault is not clearly understood. It has been named domain pipe because of the appearance and

complementary contrast. It is observed in this work that the domain pipes lie on the fault plane and the diameter of the pipe in two dimensions is determined by the separation of the two interfaces where structure gets inverted across one and turns to normal across the other. It may be argued that the inverted contrast that comes out of the domain pipe region may be because of the existence of a pair partial dislocations along the fault plane. However, the separation that has been observed scales upto 0.5 μm which is inconsistent keeping in mind the stacking fault energy of GaN. Inversion domain pipe can be suggested as a morphological variant of inversion domain. In case, inversion domain pipe is truly a pipe, then the interface is curved with varying radius of curvature. Atomic structure model of such interface is not known and a lot of work needs to be done in that direction.

Complicated structures of inversion domain pipes pose interesting questions regarding the microscopy techniques used to characterize them. As the structure and lay out of many inversion domains is not clearly understood, it is often difficult to tilt them edge-on in order to resolve the atomic structure across the boundary and it will require simulation which in turn calls for a clear understanding of the atomic structure. By far convergent beam diffraction and diffraction contrast imaging techniques have been widely used to characterize the inversion domain boundaries. In both the cases opposite non-centrosymmetric reflections are used to produce complimentary images. It is important to note that the extinction length changes with reflection, and image contrast depends on the deviation parameter and the thickness of the sample. Careful tilting experiment may reduce the effect of deviation parameter, although that may not end up in producing exact complementary images. In this light, characterization of inversion domain boundaries by contrast reversal technique remains qualitative.

In this context it would be worthwhile to compare APB and IDB. In metallic and non-ionic solids, atomic positions do not matter, and change in atomic position which can be described by a lattice translation, leads to APB. Several such domains can be generated in metallic and non-ionic compounds. In case of ionic solids such translations are restricted as nearest neighbors play an important role and interfacial energy substantially rises if two similarly

charged ions come close to each other. Therefore, an auxiliary translation often becomes necessary in order to minimize the interfacial energy in ionic solids. In this regard APB and IDB are structurally related, the difference is that IDBs occurs in some special ionic crystals where directionality of bonds exist. The stacking mismatch boundaries may be considered as a sub-class of IDB where either the anions or the cations change the sub-lattice, as has been proposed in Holt model. APBs and IDBs can be defined as an introduction of local translation symmetry in the crystal. In diffraction contrast imaging this translation vector is recognized by the electron beam and contrast is generated. A lot of work needs to be done to quantitatively understand the contrast.

Conclusions

This study demonstrates that interfaces other than $10\bar{1}0$ may exist in wurtzite GaN. The atomic structures of such interfaces need to be understood in order to tailor properties. Inversion domain pipes are similar to inversion domains but the inversion occurs over a small volume of the crystal. Mechanism of contrast generation under two beam conditions from inversion domain pipes when they lie on a fault plane has been proposed.

Using GaN as an example, the authors have taken an attempt to explain the complexity of the problem. Similar interfaces are observed in ZnO, AlN etc. and dopants are believed to play a significant role in determining the interface chemistry. By diffraction contrast imaging, it has been shown that interfaces apart from $10\bar{1}0$ may exist across which contrast reversal takes place. However, extensive microscopy work, preferably based on other techniques is required to prove that it is truly inversion domain boundary. At this moment there is no such structural model that can explain inversion domain boundaries along other interfaces. As it appears in the present study, inversion domain pipes in two dimensions appears to be similar to inversion domain boundaries where two boundaries lie very close to each other. In case it is a pipe with curved interface and with variable radius of curvature, a structural model has to be proposed in order to resolve the structure microscopically. So long the interface structural models are not ready,

high resolution microscopy is not going to be useful. It is not possible to simulate such interfaces also in the absence of a structural model. Focal series reconstruction or iterative reconstruction of exit plane waves may yield some results. It has not been tried out so far and imaging nitrogen is also not quite easy. At the end, the authors would like to conclude that understanding such interfaces would require extensive interface modeling and microscopy work which is far from complete.

Acknowledgement

Authors would like to acknowledge Prof. C. Barry Carter, University of Connecticut, USA with whom the authors spent quite long time as Post Doctoral Fellows and the work was initiated during that time. JB would like to acknowledge the stimulating discussions on various occasions with Prof. R. C. Pond, University of Liverpool, UK and Prof. I. P. Jones, University of Birmingham, UK on this subject. Discussion with Dr. S. Kumar, Intel Research & Development Center, Portland, Oregon, USA is thankfully acknowledged.

References

- [1] V. Potin, P. Ruterana, G. Nouet, *Mater. Sci. Engg.*, B59, 173-176, (1999).
- [2] D. J. Smith, D. Chandrasekhar, B. Sverdlov, A. Botchkarev, A. Salvador, H. Morkoc, *Appl. Phys. Lett.*, 67(13), 1830-1832, (1995)
- [3] S.N. Basu, T. Lei, T. D. Moustakas, *J. Mater. Res.*, 9(9), 2370-2378, 1994.
- [4] D.Cherns, W. T. Young, F. A. Ponce, *Mater. Sci. Engg. B*, 50, 76-81, (1997).
- [5] V. Potin, G. Nouet, P. Ruterana, *Appl. Phys. Lett.*, 74(7), 947-949, (1999)
- [6] P. Ruterana, J. Chen, G. Nouet, *Mater. Sci. Engg. B*, 82, 123-127, (2001).
- [7] J. E. Northrup, J. Neugebauer, L. T. Romano, *Phys. Rev. Lett.*, 77(1), 103-106, 1996
- [8] S. B. Austerman, W. G. Gehman, *J. Mater. Sci.*, 1, 249, (1966)
- [9] D. B. Holt, *J. Phys. Chem. Solids*, 30, 1297, (1969).
- [10] V. Potin, P. Ruterana, G. Nouet, *J. Appl. Phys.*, 82(5), 2176-2183, 1996

Battery (Management & Handling) Rules 2001 - An Update & Way Forward

L. Pugazhenthly

Past President, IIM & Executive Director, India Lead Zinc Dev Assn

Introduction

Lead batteries have become an integral part of our daily lives and its usage is increasing worldwide over the years in diverse sectors like transport, telecom, energy, IT, services etc., India has been witnessing double digit growths in the battery sector due to the expansions in automobiles, invertors, UPS etc., At the same time, the battery which contains lead metal as well as sulphuric acid, has health &

environmental implications, because of the associated harmful effects.

In order to encourage safe and best practices in dealing with lead batteries, the Ministry of Environment & Forests brought out a legislation “**Battery (Management & Handling) Rules 2001**”. This article sums up a current update on this important legislation and also suggests a way forward, for effective implementation, towards environment–friendly recycling.



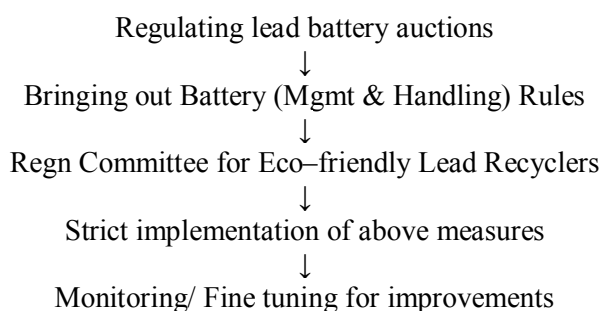
Origin

From the sixties, India was recycling used lead batteries, though very small quantities, in a crude manner, with low recoveries and more emissions, due to lack of appropriate technologies as well as environmental awareness. Because of the serious

environmental and health risks, the Supreme Court of India banned imports of used lead batteries and other hazardous wastes. As a result the lead battery sector as well as the lead industry were in doldrums affecting transport, power, telecom, defence etc.,

In order to retrieve the ailing industry, ILZDA organized an “**International Conference on Lead**

& Zinc Recycling” at Delhi on 17&18 Dec 1998. The conference deliberations gave birth to the formation of a CORE GROUP (MoEF, CPCB, CII, ILZDA, Ministry of Mines, Ministry of Industry & Indian Battery Manufacturers Assn). The Core Group, after a series of deliberations, decided to create an appropriate framework for ensuring a “close loop” arrangement for collection and environment–friendly recycling of used lead batteries.



In the earlier days, the auctions were attended by metal traders, scrap merchants etc., and they were picking up the used batteries and feeding backyard recyclers. Therefore, the above regulation insisted that only registered/ authorized lead recyclers could participate in the auctions (dissuaded the middlemen) so that the recyclables go to the eco–friendly recycling units only.

The Battery (Management & Handling) Rules 2014 covered all stakeholders ie., manufacturers, dealers, importers (of new batteries), battery assemblers, reconditioners, auctioneers, individual consumers and bulk consumers; the main aim is to collect the old battery against the sale of the new battery on a “**one-to-one**”– basis and to ensure that they are processed by registered eco–friendly lead recyclers only. B(M&H)R also mandated that battery manufacturers and dealers should file returns with the SPCBs on the no. of batteries collected; SPCBs should send these returns to the MoEF so that there is a clear picture on the national inventory. The B(M&H)R also encouraged setting up collection centres across the country for used lead batteries. The battery collection targets fixed in the rules are:

I Year (2002)	: 50%
II Year (2003)	: 75%
After III Year	: 90%

Ultimately India should collect 100% used lead batteries back and send them for environment–friendly recycling only.

The Regn Committee consisting of experts from the industry, MoEF, CPCB, ILZDA, scientific institutions etc., used to go through the applications of lead recyclers, visit the plants for effecting improvements and finally gave registration/ authorization to such eco–friendly units.

Even after the implementation of the B(M&H)R, the backyard lead recyclers were thriving and active because the battery dealers were diverting the collected batteries to the traders and backyard recyclers. In order to control this trend, the battery dealers in the country were asked, through an amendment in 2010, to get themselves registered with the respective State Pollution Control Boards and to file returns. The returns would indicate the no. of collected batteries and also its pathway ie., they are being sent to registered environment–friendly recyclers only.

Likewise all the importers of new lead batteries were also mandated, through the same amendment in 2010, that they should also get registered with the State Pollution Control Boards and file returns providing info on the no. of batteries imported and sending the collected old batteries to the registered lead recyclers only.

In the same year 2010, the Registration Committee on Hazardous Wastes was shifted from CPCB to the State Pollution Control Boards, for implementation.

Since then, the collection and recycling of used lead batteries received serious setbacks and currently one is not happy with the state of affairs. All the good work done in the earlier years has vanished and backyard recycling is active once again.

Way Forward

India has a limited capacity for primary lead production (Hindustan Zinc Ltd, 185000 tonnes per year). The Lead Demand as, per the Planning Commission, for the year 2013-14 is 464000 tonnes and this is bound to go up to 568000 tonnes by 2016-17. The unofficial lead demand is much higher. In any case, even with the official lead demand figure, there is a huge demand–supply gap and this is the opportunity that exists for recycled lead.

The country introduced excellent initiatives for an organized collection and environment-friendly lead battery recycling. We should take them to logical conclusions by taking the following measures:

- Strict enforcement/ monitoring by SPCBs
- Focus dealers & importer
- Tighten backyard smelting
- Encourage collection centres

- Stringent customs clearance
- Continue awareness program
- Introduce cleaner recycling technologies
- Implement occupational exposure precautions

The above measures should make India a country adopting “**Sustainable Development**” in the lead industry in letter and spirit.

Metallurgy Society, BHU

The Metallurgy Society, BHU, known among its membership as METSOC has been actively functioning since 1963.

The aims and objectives of the "Metallurgy Society" are:

1. To develop the art of speaking amongst students.
2. To keep abreast of developments in Metallurgical Engineering and allied subjects,
3. To foster social and cultural life amongst members,
4. To provide a platform for distinguished visitors including alumni.

The functions of the society are:

1. To arrange for the presentation of papers of technical as well as general importance,
2. To arrange symposia on subjects of interest,
3. To arrange meetings to welcome or bid farewell.
4. To create meetings to felicitate postgraduates,
5. To organize Social and Cultural activities like film-shows, excursions etc.

The membership of the society:

All students, research scholars and members of teaching staff of the Department of Metallurgical Engineering, Indian Institute of Technology (Banaras Hindu University), are ipso facto members of the Society. Membership is also open to any others interested in the activities of the society subject to the approval of the Executive.

GENERAL BODY:

The General Body, consisting of all the members of the Society, will be the supreme authority of the Society. It will hold its meetings in the Department of Metallurgical Engineering unless otherwise decided by the Executive or the President.

The Metallurgy Society is a very vibrant society. Every year, the society organises several activities with the active participation of the students and faculty members. These activities are organised in close association with the Varanasi Chapter of the Indian Institute of Metals, Kolkata and also its Students Affiliate Chapter. These activities include

1. Organization of lectures by eminent visiting scientists and engineers
2. Organization of Quizzes, Industrial visits.

Another major annual feature of the student activities of the society is the organisation of "Anveshan", a national level gala event of co-curricular activities such as technical paper presentation contest, model exhibition, etc.

On the extra-curricular front, students enthusiastically organise several Maitri-Shield matches between the teachers' team and out-going students' team. Activities such as Picnics, Diwali-Milan, Holi-Mialn etc. are also organised in order to foster social interaction among teachers and students.

CONTENTS

Displacements Caused by the Growth of Bainite in Steels <i>H.K.D.H. Bhadeshia</i>	...	1
Challenges in Technology for Processing Amorphous Fe ₈₀ B ₂₀ Alloy Ribbons Using Planar Flow Melt Spinner <i>Bhaskar Majumdar, D Arvindha Babu And S.V. Kamat</i>	...	9
Effect of Cryorolling and Ageing on Microstructure, Mechanical Properties and Corrosion Behavior of Al-Cu-Mg-Si Alloy <i>P. Nageswara Rao, M. Gopi and R. Jayaganthan</i>	...	19
Strain Hardening in Ferritic Steels <i>Santosh Kumar and D.S. Sarma</i>	...	29
Quantitative Failure Analysis <i>P. Parameswaran, E. Mohandas and M. Vijayalakshmi</i>	...	35
Microstructure Based Design of Formable Steels <i>P.P. Chattopadhyay</i>	...	43
Quasicrystal: Bulk to Nano <i>T.P. Yadav, N.K. Mukhopadhyay and O.N. Srivastava</i>	...	53
Interface Structure of Inversion Domain Boundary: A Case Study on Polycrystalline GaN <i>Joysurya Basu and R. Divakar</i>	...	65
Battery (Management & Handling) Rules 2001 - An Update & Way Forward <i>L. Pugazhenthly</i>	...	73